

# LARGE-SCALE SIMULATIONS OF PHASE TRANSITIONS AND LOW-DIMENSIONAL MAGNETS

G. KAMIENIARZ

Institute of Physics, Adam Mickiewicz University  
ul. Umultowska 85, 61-614 Poznań, Poland  
e-mail: gjk@pearl.amu.edu.pl

## Abstract

Recent developments in computer simulations of phase transitions in Ising-like systems and thermodynamic behaviour of quantum spin chains are reviewed. A combination of stochastic Monte Carlo as well as deterministic transfer matrix and finite-size diagonalization methods is described in both fields as regards static properties. Asymptotic analysis and extrapolation techniques are presented in detail. Some effective-field methods, series expansions, spin dynamics simulations and experimental applications are also discussed.

## 1 Introduction

Phase transitions and critical phenomena have been the subject of intense study for a few decades. It has led to the concept of universality, scaling invariance and the idea of a small number of critical exponents. Only a limited number of exact solutions has been found so that main results are based on approximate solutions (such as series expansions and renormalisation group theory) and numerical techniques.

Recent progress in computer technology and development of new algorithms for Monte Carlo simulations together with new methods (Landau, 1994) of analysis have yielded results of high resolutions competing with the series expansion and renormalisation group data.

The role of computer simulations in the field of low-dimensional quantum spin systems has also increased since the pioneering work of Bonner and Fisher (1964). Particularly interesting are the applications to some soliton-bearing and Haldane-gap systems.

For a classical system one can describe the states of the system and their energies in terms of a single set of variables, like the  $z$ -components of the spin in the Ising model. Each configuration of the variables appears with the Boltzmann

probability and the problem is to sample the configurations according to the Boltzmann distribution.

Generalization of the Monte Carlo technique to quantum mechanical problem is not an easy task. In this case the states and energies are the eigenstates and eigenvalues of Hamiltonian operator acting on the Hilbert space. In many cases it is even not possible to describe exactly these eigenstates.

This article is not intended to be exhaustive. It is rather aimed at reviewing simulation studies the author has been involved in. The report is organized as follows. In Section 2 some simulations methods are described and in Section 3 the numerical analysis of simulations is discussed. Selected results for some classical and quantum systems are presented in Section 4. The report is closed with some conclusions.

## 2 Methods of simulations

### 2.1 Classical Monte Carlo

This method is applied here to the three dimensional ferromagnetic Ising model with the Hamiltonian

$$H = -J \sum_{\langle i,j \rangle} \sigma_i \sigma_j \quad (1)$$

where the spin  $\sigma_i = \pm 1$ , the sum runs over all nearest-neighbour pairs and the periodic boundary conditions are imposed.

Traditionally, Monte Carlo simulations were performed using the single spin-flip method of Metropolis which becomes rather inefficient near phase transitions due to critical slowing down. To improve the performance, the multispin coding method was devised but it did not eliminate critical slowing down (Landau, 1994). Only recently a number of cluster-flipping methods accomplished its significant reduction. Swendsen and Wang (1987) found an algorithm based on a theorem mapping the Potts model into a percolation model. At first an initial spin system is split into a set of correlated clusters and then it is flipped randomly with probability 1/2. Further improvement is due to Wolff (Wolff, 1989). According to this approach, a single cluster is growing at first and then it is flipped. In our simulations (Blöte and Kamieniarz, 1993) the cluster methods are applied.

### 2.2 Transfer matrix

The transfer matrix method is a powerful tool of simulations. In the case of an Ising-like model located on a square lattice  $L_X \times L_Y$  with periodic boundaries and nearest-neighbour interactions the transfer matrix is introduced as follows

(Kamieniarz and Blöte, 1993a). The spins belonging to the  $j$ th column are denoted by  $\vec{S}_j = (S_{j1}, S_{j2}, \dots, S_{jL_y})$  so that

$$Z = \sum_{\vec{S}_1, \dots, \vec{S}_{L_x}} \exp[-\beta \mathcal{H}(\vec{S}_1, \dots, \vec{S}_{L_x})] = \text{Tr } \mathbf{T}^{L_x} \quad (2)$$

where the transfer matrix  $\mathbf{T}$  is defined in the  $2^{L_y}$  - dim manifold of all configurations of  $L_y$  spins

$$S_{jk} = \pm 1, \quad k = 1, \dots, L_y \quad (3)$$

The transfer matrix  $\mathbf{T}$  can be split into a product

$$\mathbf{T} = \mathbf{T}_v \mathbf{T}_h \quad (4)$$

where

$$\mathbf{T}_v(\vec{S}_i, \vec{S}_j) = \exp\left[\sum_{k=1}^{L_y} (K_y S_{jk} S_{j,k+1} + h S_{ik})\right] \delta_{\vec{S}_i, \vec{S}_j}$$

is diagonal, whereas

$$\mathbf{T}_h(\vec{S}_i, \vec{S}_j) = \exp\left(K_x \sum_{k=1}^{L_y} S_{ik} S_{jk}\right) \quad (5)$$

is non-diagonal and can be expressed as a product of sparse matrices.

The transfer matrix enables not only evaluation of the partition function but also the magnetization moments which enter the Binder cumulant (Binder, 1981). From the expansion

$$Z(h) = \sum_{k=0}^{\infty} \frac{h^k}{k!} Z_k, \quad (6)$$

where

$$Z_k = \left( \frac{\partial^k Z}{\partial h^k} \right)_{h=0}, \quad (7)$$

the corresponding moments of the magnetization can be expressed as

$$\langle M^k \rangle_{h=0} = Z_k / Z_0. \quad (8)$$

To calculate accurately the lower order moments (8), it suffices to find the corresponding coefficients  $Z_k$  within a perturbative scheme, *i.e.* to expand the diagonal matrix  $\mathbf{T}_v$ , in terms of  $h$  and to keep track of the powers of  $h$  during successive multiplications of a given vector by  $\mathbf{T}$ .

### 2.3 Quantum Monte Carlo and transfer matrix

The finite-temperature quantum Monte Carlo (*QMC*) method has been applied (Suzuki, 1993) to a number of 1-dim and 2-dim spin systems. Here we consider 1-dimensional chains described by the anisotropic Heisenberg Hamiltonian with nearest - neighbour interactions (Cullen and Landau, 1983; Kamieniarz, Mallezie and Dekeyser, 1988)

The starting point of *QMC* method is the generalized Trotter formula for the exponential of a sum of  $k$  noncommuting operators

$$\exp\left(\sum_{i=1}^k \hat{\theta}_i\right) = \lim_{m \rightarrow \infty} \left[ \prod_{i=1}^k \exp\left(\frac{\hat{\theta}_i}{m}\right) \right]^m, \quad (9)$$

where  $m$  is an integer referred to as the "Trotter index".

One can apply this formula to the partition function and map a given 1d quantum model into a classical 2d system which can be studied using classical Monte Carlo or transfer matrix methods. The mapping is accomplished in the following way. The partition function  $Z$  is expressed in terms of all the eigenstates of the spin chain and the Hamiltonian is partitioned into a sum of two-body operators

$$H = \sum_{n=1}^N H_{n,n+1} = H_{odd} + H_{even} \quad (10)$$

where

$$H_{odd(even)} = \sum_{n=odd(even)} H_{n,n+1} \quad (11)$$

In the checker-board decomposition (*CBD*) (Kamieniarz *et al.*, 1988) the Hamiltonian is split into two parts  $\hat{H}_{odd}$  and  $\hat{H}_{even}$ , containing the two-body operators with odd and even  $n$ , respectively. The  $m$ th-order approximant to the partition function is then given by

$$Z_{CBD}^{(m)} = \text{Tr} \left[ \left( \hat{L}_{odd} \hat{L}_{even} \right)^m \right] \quad (12)$$

where

$$\hat{L}_{odd(even)} = \prod_{n=odd(even)} \exp\left(-\frac{\beta}{m} H_{n,n+1}\right) \quad (13)$$

By introducing the complete sets of states

$$|\sigma_r\rangle = |S_{1r}, S_{2r}, \dots, S_{Nr}\rangle \quad (r = 1, 2, \dots, 2m) \quad (14)$$

one gets

$$Z_{CBD}^{(m)} = \sum_{\sigma_1, \dots, \sigma_{2m}} \langle \sigma_1 | \hat{L}_{odd} | \sigma_2 \rangle \langle \sigma_2 | \hat{L}_{even} | \sigma_3 \rangle \dots \langle \sigma_{2m} | \hat{L}_{even} | \sigma_1 \rangle \quad (15)$$

where

$$\prod_{n=\text{odd}(\text{even})} \langle S_{nr} S_{n+1,r} | \exp\left(-\frac{\beta}{m} H_{n,n+1}\right) | S_{n,r+1} S_{n+1,r+1} \rangle = \prod_{n=\text{odd}(\text{even})} e^{-\beta E_{n,r}} \quad (16)$$

and  $r$  is odd (even) for  $\hat{L}_{\text{odd}}(\hat{L}_{\text{even}})$ . This leads to the expression for a classical partition function

$$Z_{CBD}^{(m)} = \sum_{\sigma_1, \dots, \sigma_{2m}} \prod_{\langle n,r \rangle} e^{-\beta E_{n,r}} \quad (17)$$

for a  $2d$  lattice of size  $N \times 2m$ , where  $\langle n, r \rangle$  indicates that  $n$  and  $r$  are both odd or both even. Because of the trace in  $Z$ , we have periodic boundary conditions in the Trotter direction. Imposing the periodic boundary conditions on the chain direction, the  $2d$  lattice consists of  $N \times m$  blocks of four spins ("vertices") (Kamieniarz *et al.*, 1988) and the quantity

$$W_{nr} = e^{-\beta E_{n,r}} \quad (18)$$

is called the weight of the vertex.

In the real-space decomposition (*RSD*) (Kamieniarz *et al.*, 1988) one applies the Trotter formula to the partition function using the representation  $\hat{H} = \sum_{n=1}^N H_{n,n+1}$ . Again a partition function of a classical spin - 1/2 Ising system on a  $2d$  lattice with  $N \times m$  vertices is obtained.

## 2.4 Finite-size diagonalization

Exact calculations on small finite-size lattices are considered an important complement to and a test of computer simulations on larger lattice systems (Manousakis, 1991). Although limited to substantially smaller sizes, they do not encounter such possible sources of errors in simulation studies as the Trotter approximation or metastability in Monte Carlo sampling.

The calculations proceed as follows (Bonner *et al.*, 1964; Blöte, 1975). The matrix representation of a given spin Hamiltonian is found and diagonalized numerically for finite chains with size  $N$  up to  $N_{\text{max}}$  and free boundary conditions. For a given size, interesting thermodynamic functions are then evaluated according to statistical mechanics.

## 2.5 Spin dynamics

An interest in dynamics of the ferromagnetic easy-plane Heisenberg chains stems from spin solitons (Mikeska, 1978) predicted theoretically for the *1d* model in

the symmetry breaking field which can be mapped under certain approximations onto the classical sine-Gordon model, yielding nonlinear excitations. In a reliable computer experiment with all microscopic parameters controlled and all polarizations directly measured, new insight into the validity of the sine-Gordon model can be expected (Gerling and Landau, 1990).

The dynamics of models with continuous degrees of freedom can be derived directly from equations of motion (Grille, Kamieniarz and Gerling, 1992). In the first stage a standard importance sampling Monte Carlo technique is used to generate equilibrium spin configurations for particular values of  $T$  and  $B$  with chain length of typically  $N = 20000$  sites and periodic boundaries. Next the coupled nonlinear equations of motion for the spin variables are accurately integrated up to time  $t_{max} = 100/J$  with a time integration interval  $\Delta = 0.01/J$ . For each time integration, the time and space dependent spin-spin correlation functions

$$\langle S_i^\alpha(0)S_{i+r}^\alpha(t) \rangle = \frac{1}{N} \sum_{i=1}^N S_i^\alpha(0)S_{i+r}^\alpha(t) - \langle S_i^\alpha(0) \rangle^2 \quad (19)$$

are calculated and averaged over the 10 starting configurations. Finally, the time and spatial Fourier transforms are evaluated to yield the dynamic structure factors  $S(q, \omega)$ , where  $(= x, y, z)$  denotes polarization. The same technique is also reviewed by Landau (1994) in relation to the critical dynamics simulations.

### 3 Methods of analysis

#### 3.1 Finite-size scaling

We consider a system with finite-size parameter  $L$ , e.g. a hypercube of size  $L^d$  with toroidal boundary conditions. In the vicinity of a renormalisation fixed point, the parameters describing the system include the temperature field  $t$ , the magnetic field  $h$  and the finite-size field  $1/L$ . Neglecting the irrelevant fields and nonlinearities, the asymptotic finite-size scaling relation for the singular part of the free energy per spin (Privman and Fisher, 1984; Barber, 1983) can be written as

$$f^{(s)}(t, h, 1/L) = b^{-d} f^{(s)}(tb^{y_t}, hb^{y_h}, b/L) \quad (20)$$

where  $b$  is the rescaling factor, and  $y_t$  and  $y_h$  are the bulk thermal and magnetic exponents, respectively. This finite-size scaling relation has been widely applied in numerical studies of critical phenomena and in analysing experimental data. Choosing  $b = L$ , differentiating  $k$  times with respect to  $h$  and putting  $h = 0$ ,

$$f^{(s),k}(t, 0, 1/L) = L^{ky_h - d} f^{(s),k}(tL^{y_t}, 0, 1) \quad (21)$$

The scaling function on the right hand side represents a system far from criticality (the finite-size parameters has the value 1) and is therefore assumed analytic, and may be Taylor expanded in  $tL^{y_t}$ . Expressing the magnetization moments ( $M^k$ ) in derivatives of the free energy, neglecting the analytic part, one shows that these moments obey the same scaling behaviour as above. Thus, in the vicinity of the fixed point ( $L$  large,  $t$  small) the ratio

$$Q_L \equiv \langle M^2 \rangle_L^2 / \langle M^4 \rangle_L \quad (22)$$

satisfies

$$Q_L(t) = Q + a_1 t L^{y_t} + a_2 t^2 L^{2y_t} + \dots \quad (23)$$

where  $Q$  and  $a_i$  are unknown parameters.

Another unknown is the critical temperature  $T_c$  which enters via  $t \sim T - T_c$ . The unknowns can be determined by fitting (23) to the Monte Carlo data. If  $Q$  is known, one unknown parameter is eliminated, so that the critical point can be obtained more accurately.

The finite-size scaling relation has to be modified (Kamieniarz *et al.*, 1993a) for the  $2d$  Ising model which is particular in some respects. Firstly, the specific heat singularity has a logarithmic divergence so that the zero-field free energy should contain explicitly a logarithmic term (Niemeijer and van Leeuwen, 1976). Secondly, it has been argued (Aharony and Fisher, 1983) that the leading corrections to scaling are analytic and can be accounted for by nonlinearities of the scaling fields  $g_t$  and  $g_h$  related to the thermal field  $t$  and the ordering field  $h$ . It can be arranged that the renormalisation equations which are nonlinear in  $t$  and  $h$ , become linear in variables  $g_t$  and  $g_h$ . Thus under rescaling by a factor of  $b$

$$g'_t = b^{y_t} g_t, \quad g'_h = b^{y_h} g_h \quad (24)$$

where the primes denote the renormalised quantities. Furthermore, we have for the finite-size field

$$1/L \rightarrow 1/L' = b/L,$$

so that for the  $2d$  Ising model, which has  $y_t = 1$ , the fields  $g_t$  and  $1/L$  fulfil the same relation. Their ratio  $g_t L$  is invariant under rescaling and, along a trajectory with constant  $g_t L$  one may combine  $g_t$  and  $1/L$  into a single field proportional to  $1/L$ , keeping in mind that the critical amplitudes may still depend on  $g_t L$ .

Along this trajectory the known results (Aharony *et al.*, 1983) for the scaling behaviour of the free energy in terms of  $g_t$  and  $g_h$  can be generalized and the corresponding singular part  $F^{(s)}$  of the total free energy is thus expressed as

$$F^{(s)}(g_t, g_h, L^{-1}) = A(g_t L) \ln L + B(g_t L, g_h L^{y_h}) \quad (25)$$

where  $A$  and  $B$  are unknown amplitudes and the nonlinear fields are expanded as

$$\begin{aligned} g_t &= t + b_t h^2 + c_t t^2 + \dots \\ g_h &= h(1 + c_h t + d_h t^2 + e_h h^2 + \dots) \end{aligned} \quad (26)$$

The scaling form of the free energy enables the calculation of derivatives with respect to the field at the critical point  $t = 0$ ,  $h = 0$ . From the relations

$$\langle M^2 \rangle = \frac{\partial^2 F}{\partial h^2}, \quad \langle M^4 \rangle = \left[ \frac{\partial^4 F}{\partial h^4} + 3 \left( \frac{\partial^2 F}{\partial h^2} \right)^2 \right] \quad (27)$$

we obtain (Kamieniarz *et al.*, 1993a) the following expansion for  $Q_L$  up to  $L^{3-4y_h}$ :

$$\begin{aligned} Q_L &= Q + \beta_0 L^{2-2y_h} (1 + \beta_1 L^{-1} + \beta_2 L^{2-2y_h} + \beta_3 L^{-2} + \\ &\quad \beta_4 L^{1-2y_h} + \dots) + \gamma_0 L^{1-2y_h} \ln L (1 + \gamma_1 L^{2-2y_h} + \dots) \end{aligned} \quad (28)$$

This expansion contains not only a number of algebraic powers, but also logarithmic terms which may complicate the determination of  $Q$  from the finite-size results.

### 3.2 Conformal invariance

Conformal invariance can be exploited to relate the properties of spin models on strips of finite width  $L$  and infinite length with periodic boundary conditions to those of the corresponding  $2d$  system. A relation derived by Cardy (1987) applies to the finite-size amplitude of the correlation length

$$\lim_{L \rightarrow \infty} \frac{L}{\xi_i} = 2\pi x_i \quad (29)$$

where  $x_i = d - y_i$  is the anomalous dimension of the observable associated with the correlation length. The scaled gaps

$$Lg_i(L)/2\pi \quad (30)$$

where

$$g_i(L) = \xi_i^{-1}(L) = \ln \frac{\lambda_0}{|\lambda_i|} \quad (31)$$

provide estimates of  $x_i$  which can be evaluated from power-law extrapolations.

### 3.3 Finite-size extrapolations

Estimates of thermodynamic quantities for macroscopic systems can be found from the finite-size data  $A_{N_j}$  by recourse to extrapolation procedures (Bonner *et al.*, 1964; Blöte, 1975; de Neef, 1976). The series  $A_N$  have been mainly analysed in terms of polynomial expansions. These methods assume (Campana, Caramico D'Auria, Esposito, Kamieniarz and Dekeyser, 1990) that the  $A_n$  may be approximated by expressions of the form

$$A_N \simeq A_N(n) = \sum_{k=0}^n B_k y_N^k, \quad (32)$$

where  $y_N$  are obtained by minimizing the mean square deviation

$$\Delta^2 = \sum_{N=N_1}^{N_2} [A_N - A_N(n)]^2 / M, \quad M = N_2 - N_1 + 1, \quad (33)$$

and  $y_N = f(1/N)$ , with a function  $f(x)$  fulfilling the property  $f(0) = 0$ . The parameter  $B_0$  is clearly the estimate for  $A$  in these methods. Apart from the magnitude of  $\Delta^2$ , the quality of this analysis can be estimated from the rate of convergence obtained for  $B_k$  when the lowest index  $N_1$  is changed.

The polynomial extrapolations usually performed, correspond to the choice  $y_N = 1/N$ . Because of the limited number of  $A_N$  values, the results may not be improved by increasing the order  $n$  of the polynomial as the higher-order coefficients  $B_k$  do not always remain small. In practice, the series have been analysed by linear ( $n = 1$ ) and quadratic ( $n = 2$ ) fits.

Obvious choices are also simple powers  $f(x) = x^\alpha (\alpha > 0)$ , or  $f(x) = 1/\ln(x)$ . One tries to obtain a better convergence by first transforming the variable  $1/N$  into  $y_N = f(1/N)$  and then by fitting the  $A_n$  data to a low-order polynomial of the form (32). In our analysis (Campana *et al.*, 1990) however, the best results in terms of acceptable estimates with low  $\Delta^2$  values were obtained with the form

$$f(x) = (e^{\alpha x} - 1)/\alpha, \quad (34)$$

or  $f(x) = x/(1 - \alpha x)$ . In each case,  $\alpha$  is a free parameter again determined by minimizing  $\Delta^2$ . Although formally equivalent to the previous method (expansions in powers of  $1/N$ ), it has the advantage of allowing the incorporation of higher-order terms in a low-order expansion.

Some relations have been rigorously established for the finite-size estimates. The asymptotic form of the specific heat per site  $C_N$  calculated for the chains of size  $N$  depends on the boundary conditions (de Neef, 1976). For free boundary conditions:

$$C_N^{chain} = C_\infty - \frac{b}{N} + o(\beta^{2N+2}), \quad (35)$$

where the correction term has an alternating effect depending on the even or odd value of  $N$ , whereas for periodic boundary conditions:

$$C_N^{ring} = C_\infty + \frac{\Phi_N}{N} + O(\beta^N), \quad (36)$$

where not only the correction term is of the lower order with respect to  $N$  but also the second term depends on  $N$ . For antiferromagnetic interactions  $\Phi_N$  is alternating in sign for even and odd  $N$ , whereas for ferromagnetic exchange - it is uniform in sign.

As to the *QTM* finite- $m$  results, (Delica and Leschke, 1990) the behaviour

$$C_m = C_\infty + \sum_{n=1} \frac{a_n}{m^{2n}} \quad (37)$$

is expected.

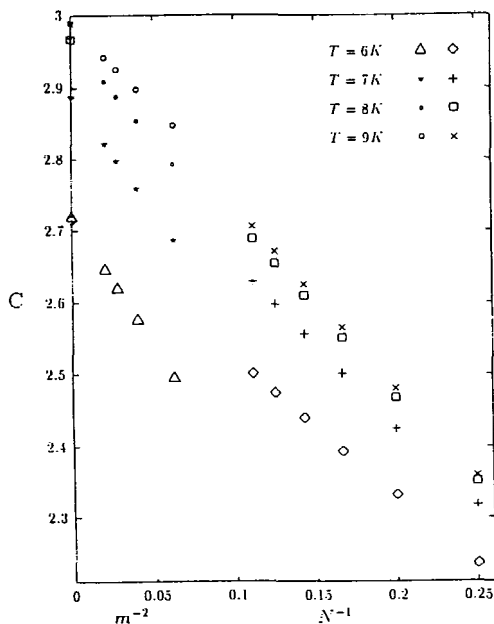


Figure 1: Variation of the zero-field specific heat  $C$  in molar units ( $J/mole K$ ) against  $1/m^2$  (the transfer matrix data,  $4 \leq m \leq 7$ ) and  $1/N$  (the finite-chain diagonalization data,  $4 \leq N \leq 9$ ). The symbols on the ordinate axis shows the corresponding extrapolated values.

The  $1/N$  and  $1/m^2$  dependence of the thermodynamic quantities in the low temperature region for the ferromagnetic  $S = 1$  easy-plane Heisenberg chain is illustrated in Figs. 1-3 for the microscopic parameters  $J/k_B = 20.5 K$  and  $A/J = 0.425$  found by Campana, Caramico D'Auria, Esposito, Esposito, Gerling

and Kamieniarz (1992a). The variation of the molar finite-size specific heat (Campana, Caramico D'Auria, Esposito, Esposito and Kamieniarz, 1996) with respect to  $1/N$  is plotted for temperatures  $6 \leq T \leq 9K$  in Fig. 1. In the entire temperature range the  $1/N$  dependence shows linear behaviour so that the extrapolated data can be extracted with the accuracy of an order of 0.1% and within this error they agree with the transfer matrix data plotted versus  $1/m^2$  in the same figure.

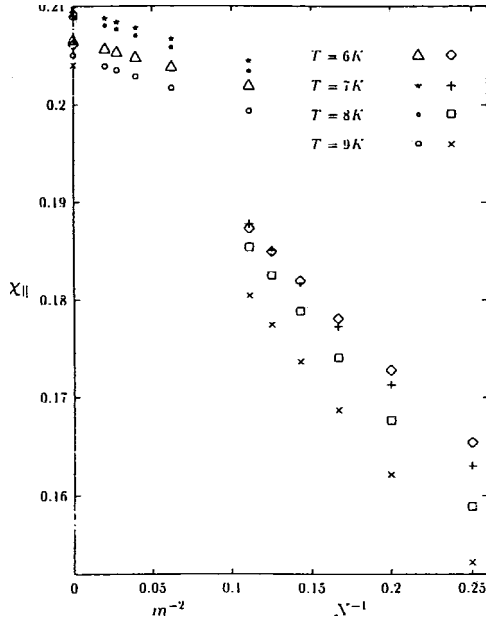


Figure 2: Variation of the longitudinal susceptibility  $\chi_{||}$  in the molar units (*emu/mole*) against  $1/m^2$  (for the transfer matrix data,  $3 \leq m \leq 7$ ) and  $1/N$  (for the finite-chain diagonalization data,  $4 \leq N \leq 9$ ). The extrapolated values are depicted on the ordinate axis.

The relation (35) refers only to the specific heat, nevertheless we also analyse (Campana *et al.*, 1996) other thermodynamic quantities in terms of the inverse length  $N^{-1}$ . As can be seen from Fig. 2, even in our low temperature region ( $T \leq 9K$ ) the linear dependence of  $\chi_{||}$  for the finite-chain data in  $1/N$  and that of the QTM results in  $1/m^2$  is well fulfilled. As to the excess specific heat  $\Delta C = C(T, B) - C(T, B = 0)$ , the corresponding size dependence is illustrated in Fig. 3.

Qualitatively the same finite-size behaviour is observed for systems with antiferromagnetic interactions. In Fig. 4 a typical size dependence of susceptibility is shown for a model of the Haldane-gap compound  $CsNiCl_3$  (Kamieniarz and

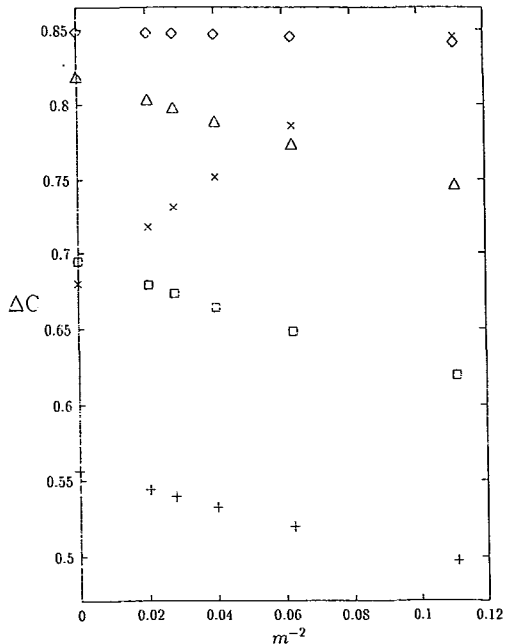


Figure 3: Dependence on  $1/m^2$  of the excess specific heat  $\Delta C$  (J/mole K) in the field  $B = 0.5$  kGs. The symbols  $\times$ ,  $\diamond$ ,  $\triangle$ ,  $\square$ ,  $+$  display the data at  $T = 6, 7, 8, 9, 10$  K, respectively. The extrapolated predictions are illustrated on the ordinate axis.

Matysiak, 1996a).

The finite-size data can also be analysed (Campana *et al.*, 1990) in the framework of the Pade approximant method. This method is based on the fact that the limit  $A_\infty$  of a series  $A_N$  can be obtained from

$$A_\infty = (1 - z)F(z) |_{z=1} \quad (38)$$

where

$$F(z) = \sum_{N=0}^{\infty} A_N z^N \quad (39)$$

so that

$$(1 - z)F(z) = A_0 + \sum_{N=1}^{\infty} (A_N - A_{N-1})z^N \quad (40)$$

From the coefficients  $A_N$  one can build Pade approximants to  $(1 - z)F(z)$  and get estimates of  $A_\infty$ . A variant of the method is the alternating  $\varepsilon$ -algorithm described by Barber (1983).

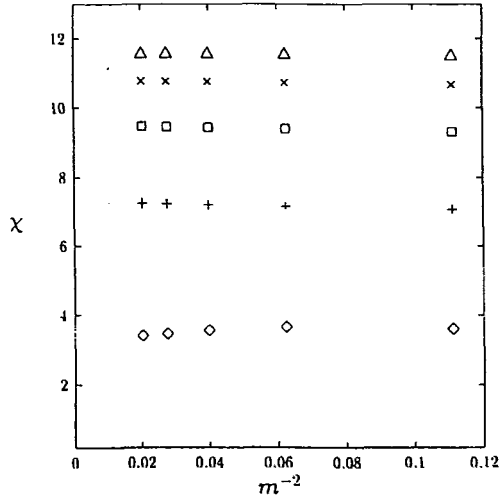


Figure 4: Variation of  $\chi_{\perp}(emu/mole)$  for negative  $J$  against  $1/m^2$  ( $3 \leq m \leq 7$ ) and  $1/N$  ( $4 \leq N \leq 8$ ). The corresponding extrapolated values are given on the ordinate axis.

Another procedure is to construct new series (Bonner *et al.*, 1964; Blöte, 1975). If the series  $A_N$  consists of a number of power-law terms  $N^{-x_i}$  ( $i = 1, 2, \dots$ ), a given power  $N^{-x}$  is eliminated (Kamieniarz *et al.*, 1993a) in the new series defined as

$$A'_N = [(N+1)^x A_{N+1} - N^x A_N] / [(N+1)^x - N^x] \quad (41)$$

In the modified series  $A'_N$  the power-law behaviour is preserved with the same constant  $A_{\infty}$ , but without the term containing  $N^{-x}$ .

### 3.4 Effective fields with correlations

A possible generalization of the mean-field approximation for a system with short-range interactions can be introduced (Dekeyser and Kamieniarz, 1992) as follows. We divide the lattice into a finite cluster  $\Omega$ , its boundary  $\partial\Omega$  and the complement  $\bar{\Omega}$ , as shown in Fig. 5. The corresponding spin degrees of freedom are denoted by the variables  $\sigma \in \Omega$ ,  $\tau \in \partial\Omega$ ,  $\bar{\sigma} \in \bar{\Omega}$ . The Hamiltonian of a system is split into the form

$$-\beta\mathcal{H}(\sigma, \tau, \bar{\sigma}) = H_0(\sigma, \tau) + H_1(\tau, \bar{\sigma}) \quad (42)$$

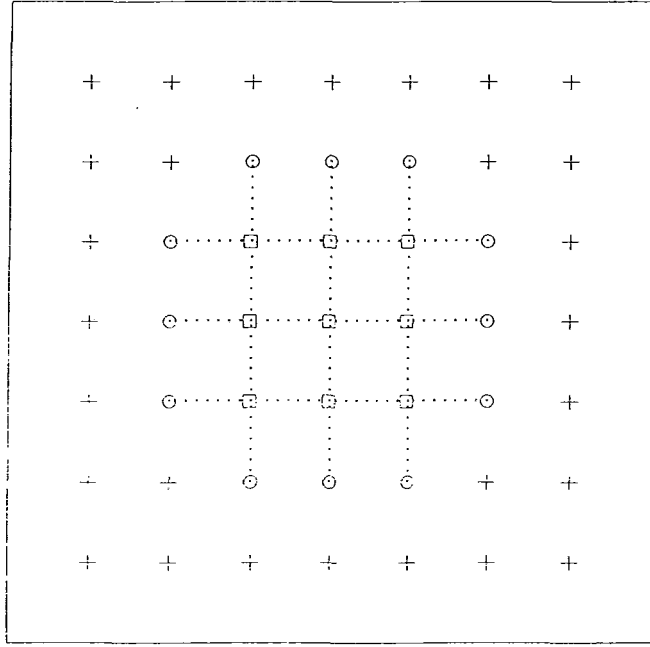


Figure 5: Partition of the lattice into the cluster  $\Omega$ , the boundary  $\partial\Omega$ , and the complement  $\bar{\Omega}$ .

and we address a problem of estimating the thermal expectation value

$$\langle A \rangle = \frac{1}{Z} \text{Tr} e^{-\beta H(\sigma, \tau, \bar{\sigma})} \quad (43)$$

For a classical system the average

$$\langle A \rangle = \frac{\sum_{\sigma\tau} A(\sigma, \tau) e^{H_0 + H'(\tau)}}{\sum_{\sigma\tau} e^{H_0 + H'(\tau)}} = \frac{\sum_{\sigma\tau} A e^{H_0} Q(\tau)}{\sum_{\sigma\tau} e^{H_0} Q(\tau)} \quad (44)$$

can be expressed in terms of the effective Hamiltonian  $H'(\tau)$ , where

$$e^{H'(\tau)} = \sum_{\bar{\sigma}} e^{H_1(\tau, \bar{\sigma})} \equiv Q(\tau) \quad (45)$$

The simplest approximation of  $Q(\tau)$  is the mean-field approximation, *i.e.* a dependence linear in  $r$  variables. However, higher order terms in  $r$  can be also imposed according to the symmetry of  $\mathcal{H}$ . These new terms contain correlations in  $r$  variables.

The function  $Q(\tau)$  can be expanded in a form (Dekeyser *et al.*, 1992)

$$Q(\tau) = \prod_i (1 + a_i \tau_i) \prod_{i \neq j} (1 + b_{ij} \tau_i \tau_j) \dots \quad (46)$$

where the coefficients  $b_{ij}$  take into account the correlations between the spins of  $\partial\Omega$ . The symmetry properties of the cluster are reflected in the symmetry properties between these coefficients.

Then a sequence of systematically improvable approximations can be worked out (Kamieniarz, Musial and Dekeyser, 1994), imposing selfconsistent conditions on the coefficients in eq.(46) for  $Q$  (in analogy with the usual mean field approximation) or implementing the renormalisation-group ideas (in analogy with the mean-field renormalisation group method (Indekeu, Maritan and Stella, 1982) denoted as MFRG) which lead to non-classical critical exponents.

The critical couplings  $K_c = J/k_B T_c$  for the Ising clusters with  $L^2$  sites on the square lattice are given in Table 1. In the second and the third column, the cluster mean-field approximation results and the original MFRG predictions (Indekeu *et al.*, 1982) are given. Performing the selfconsistent calculations (Kamieniarz, Musial and Dekeyser, 1996b) with two parameters in  $Q(r)$  for the pair correlations of  $r$ , we find the results for  $K_c$  given in the 4th and 5th columns of Table 1 for the  $Q$  and the renormalisation-group scheme, respectively. A much faster convergence is obtained by increasing the order of the approximation than by increasing the cluster size in MFA. The corresponding critical exponents  $y_t$  and  $y_h$  for the thermal and ordering fields are given in the remaining part of Table 1. The values are considerably improved, in particular the exponents  $y_t$ .

Table 1: The critical coupling  $K_c$  and the critical exponents for the  $2d$ -Ising model.

| L | MFA   | MFR   | $Q^{sc}$ | $Qrg$ | MFR   | $Q^{T9}$ | MFR   | $Qrg$ |
|---|-------|-------|----------|-------|-------|----------|-------|-------|
|   | $K_c$ |       |          |       | $y_t$ |          | $y_h$ |       |
| 1 | 0.250 |       |          |       |       |          |       |       |
| 2 | 0.286 | 0.361 | 0.412    |       | 0.69  |          | 1.50  |       |
| 3 | 0.308 | 0.381 | 0.414    | 0.409 | 0.78  | 0.972    | 1.57  | 1.69  |
| 4 | 0.323 | 0.393 | 0.417    | 0.412 | 0.82  | 0.989    | 1.60  | 1.69  |
| 5 | 0.335 | 0.401 |          |       | 0.84  |          | 1.62  |       |

The qualitatively different situation appears for quantum mechanical models. The Boltzmann factor cannot be factorized so that an effective Hamiltonian  $H'(\sigma, \tau)$

$$e^{H_0+H'(\sigma, \tau)} = \sum_{\bar{\sigma}} e^{H_0+H_1(\tau, \bar{\sigma})} \quad (47)$$

may also depend on the variables  $\sigma$  from the interior of the cluster  $\Omega$ .

We assume (Dekeyser *et al.*, 1992) that the strongest contributions to  $H'(\sigma, \tau)$  appear at or around the boundary  $\partial\Omega$  and we choose them according to the symmetry of  $\mathcal{H}$ .

For simple  $1d$  Heisenberg Hamiltonian without external field, no broken symmetry can be expected and we can argue that for symmetry reasons no external field can appear in  $H'$ . The first contribution that can be expected in  $H'$  is an extra Heisenberg interaction between the first and the second spin in a finite segment, and equally between the last and the last but one:

$$H_0 + H' = -\frac{1}{2} \sum_{i=0}^{N-1} K_i (\sigma_i^x \sigma_{i+1}^x + \sigma_i^y \sigma_{i+1}^y + \sigma_i^z \sigma_{i+1}^z), \quad (48)$$

where  $K_0 = K_N = K + D$  and  $K_i = K$  for all other  $i$ .

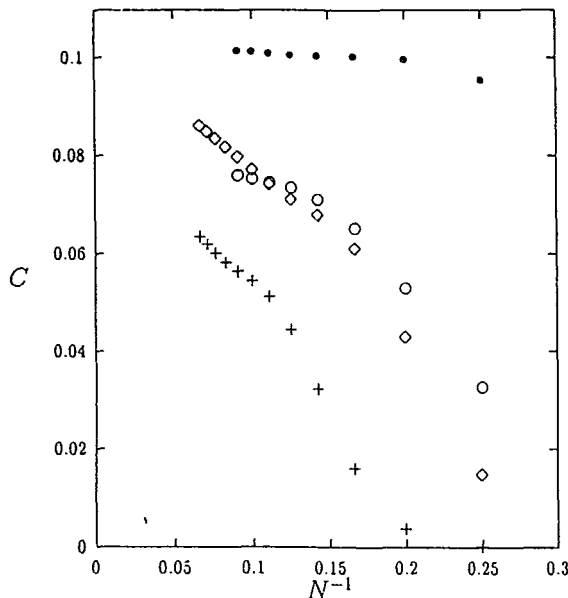


Figure 6: The finite-size results for the zero-field specific heat of the  $1d$  Heisenberg model. The symbols  $\bullet$ ,  $\diamond$  represent the standard and improved data at  $K^{-1} = 0.1$ , whereas  $\circ$ ,  $+$  – the corresponding data at  $K^{-1} = 0.05$ .

Our finite-size predictions for the zero-field specific heat in the low temperature region ( $k_B T/J = 0.10$  and  $k_B T/J = 0.05$ ) are illustrated in Fig.6, performing direct diagonalization with free boundary conditions (Kamieniarz *et al.*, 1996b). The results of the standard finite-segment calculations ( $D = 0$ ,  $N \leq 14$ ), given by  $\diamond$  symbols, reveal a strong size dependence. Assuming  $D \neq 0$  and imposing  $\langle \sigma_0^x \sigma_1^x \rangle = \overline{\langle \sigma_i^x \sigma_{i+1}^x \rangle}$ , we find that the variation in terms of  $1/N$  is significantly reduced and the data converge towards the same asymptotic value.

We consider these results encouraging and our scheme a key issue to get reliable extrapolations of the thermodynamic quantities at temperatures lower than those considered earlier (Campana *et al.*, 1990).

The standard molecular field approximation is still a valuable tool for obtaining qualitative understanding of phase diagrams whenever exact solutions are impossible. An extended Ashkin-Teller model (Pawlicki, Kamieniarz and Rogiers, 1995) belongs to that class and can be expressed in terms of spin variables  $s, \sigma = \pm 1$  as

$$\mathcal{H} = - \sum_{\langle i,j \rangle} [J s_i s_j + J' \sigma_i \sigma_j + J_4 (s_i \sigma_i)(s_j \sigma_j) + J_0] - \sum_{\langle i,j \rangle} [K (s_i + s_j)(\sigma_i \sigma_j + 1)], \quad (49)$$

Phase diagram of the original model ( $K = 0$ ) on a two dimensional lattice has been discussed by Baxter (1982). Some renormalisation group calculations (Cachine, Drugovich de Feli and Caticha, 1989) have been undertaken to obtain a more accurate description of the diagram. Exact solutions for a limited range of interaction parameters are also available (Pearce and Seaton, 1990).

We performed a numerical molecular-field analysis of the extended model, considering a bipartite lattice and the following order parameters:

$$\begin{aligned} \langle s_{1,i} \rangle &= m_1, & \langle s_{2,i} \rangle &= m_2, \\ \langle \sigma_{1,i} \rangle &= n_1, & \langle \sigma_{2,i} \rangle &= n_2, \\ \langle s_{1,i} \sigma_{1,i} \rangle &= p_1, & \langle s_{2,i} \sigma_{2,i} \rangle &= p_2, \end{aligned} \quad (50)$$

where integers 1 or 2 distinguish between different sublattices and (...) is a thermal average.

Results of our numerical analysis for the symmetric case  $J = J' > 0$  are summarized in Fig. 7, which displays a rich temperature phase diagram. The surface of phase transitions is symmetric with respect to the plane  $K/J = 0$  so that we show only a few lines corresponding to  $K/J < 0$ . Except for the areas denoted by broken lines, the critical surface consists of second order transition points. At these points only for  $K = 0$  all the order parameters simultaneously vanish. For  $K \neq 0$ , the parameters  $m_1, m_2$  remain always nonzero because  $K$  acts on spins as a magnetic field.

At point A two lines of tricritical points appear according to the symmetry. On the FM line the surface bifurcates. In a higher part (FMG and its symmetric counterpart for  $K < 0$ ) there is a jump in all the order parameters and with increasing  $J_4$  this surface turns into a single second order transition line GC. At the point H, the surface indicated by lines c begins to climb up along the line a.

For  $J_4/J < -1$  another sheet of critical surface emerges from point D with two lines of tricritical points. Again, only a line for  $K > 0$  is indicated. Two separate sheets of critical surface are joined by a single, second order transition line DH.

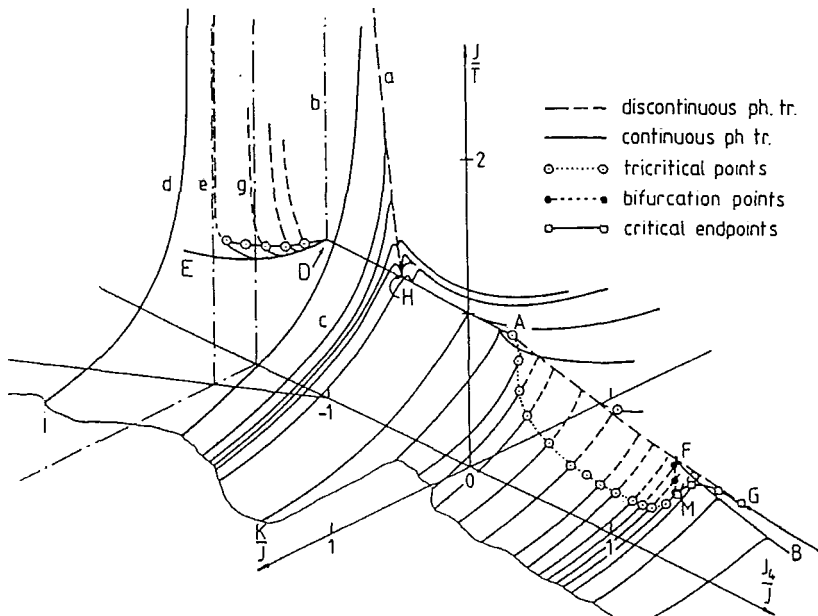


Figure 7: Phase diagram in  $J/T$ ,  $K/J$ ,  $J_4/J$  variables. Lines  $d, e, g$  are in  $J_4/J = -1.5$  plane. Lines  $a, b, EDHAFGC$  and  $FB$  are in  $K = 0$  plane.

## 4 Results of simulations

### 4.1 3d Ising model

The three-dimensional Ising model continues to be a subject of investigations, in particular its critical behaviour. Whereas the most accurate results traditionally came from series expansions (Liu and Fisher, 1989; Nickel and Rehr, 1990) and from the  $\epsilon$ -expansion (Le Guillou and Zinn-Justin, 1980), the error margins quoted in Monte Carlo based approaches are shrinking considerably (Ferrenberg and Landau, 1991; Baillie, Gupta, Hawick and Pawley, 1992). However, numerical results of such simulations are not always in a satisfactory agreement with one another. Although these differences are not large, they invite the consideration of possible sources of systematic errors such as effects due to a poor random number generator, effects introduced by histogramming methods, the use of a single row of pseudo-random numbers for a few parallel simulations or neglecting corrections to scaling in fitting procedures of simulation results.

We have simulated simple cubic Ising lattices with periodic boundary conditions and analysed the amplitude ratio

$$g_L = Q_L^{-1},$$

where  $QL$  is given by Eq.(22) and  $L$  is the linear system size. The Monte Carlo data were mainly generated using the Swendsen-Wang cluster method for  $K = 0.221653$  (Blöte *et al.*, 1993) but we also included some contributions from the largest-cluster method and Wolff algorithm (Blöte and Kamieniarz, 1994).

Table 2: Finite-size results for the universal ratio  $g_L$  of the three-dimensional Ising model. The first column shows the finite size  $L$ , and the second one our Monte Carlo data with standard errors in the last decimal place between parentheses. The next column shows the length of the simulations. The fourth column lists our exact numerical transfer matrix results, and the last one contains, for comparison, part of the numerical results of Livet.

| $L$ | $g_L$ (present) | # conf.           | $g_L$ (exact) | $g_L$ (Livet) |
|-----|-----------------|-------------------|---------------|---------------|
| 3   | 1.49599( 7)     | $1.4 \times 10^8$ | 1.496016      |               |
| 4   | 1.51565( 7)     | $1.8 \times 10^8$ | 1.515605      | 1.5167 ( 6)   |
| 5   | 1.52956(14)     | $6.4 \times 10^7$ |               |               |
| 6   | 1.54032(19)     | $4.8 \times 10^7$ |               | 1.5431 ( 6)   |
| 7   | 1.5483 ( 2)     | $4.8 \times 10^7$ |               |               |
| 8   | 1.5545 ( 2)     | $4.8 \times 10^7$ |               | 1.5572 ( 9)   |
| 9   | 1.5597 ( 2)     | $4.8 \times 10^7$ |               |               |
| 10  | 1.5636 ( 2)     | $4.8 \times 10^7$ |               |               |
| 11  | 1.5666 ( 2)     | $4.8 \times 10^7$ |               |               |
| 12  | 1.5696 ( 2)     | $4.8 \times 10^7$ |               | 1.5709 (14)   |
| 13  | 1.5722 ( 3)     | $4.0 \times 10^7$ |               |               |
| 14  | 1.5740 ( 3)     | $4.0 \times 10^7$ |               |               |
| 15  | 1.5756 ( 4)     | $2.0 \times 10^7$ |               |               |
| 16  | 1.5766 ( 4)     | $2.0 \times 10^7$ |               | 1.5791 (13)   |
| 18  | 1.5790 ( 4)     | $2.0 \times 10^7$ |               |               |
| 20  | 1.5825 ( 4)     | $2.0 \times 10^7$ |               |               |
| 22  | 1.5837 ( 4)     | $2.0 \times 10^7$ |               |               |
| 24  | 1.5857 ( 4)     | $2.0 \times 10^7$ |               | 1.5820 (25)   |
| 28  | 1.5867 ( 4)     | $2.0 \times 10^7$ |               |               |
| 32  | 1.5875 ( 7)     | $1.0 \times 10^7$ |               | 1.5943 (28)   |

The Monte Carlo data collected in Table 2 are restricted to rather small size systems ( $L \leq 32$ ), but have a greater statistical accuracy than other results known to us for these systems. We have analysed our data according to

$$g_L(K) = g + bL^{y_i} + a_1(K - K_c)L^{y_i} \quad (51)$$

with  $a_1 = 0.86$  and  $y_i = 1.59$  (Liu *et al.*, 1989; Nickel *et al.*, 1990; Le Guillou *et al.*, 1980; Ferrenberg *et al.*, 1991) in order to determine  $K_c$ ,  $y_i$  and  $g$ . A

least-square fit showed that the data for  $L = 4$  deviate significantly, and the fits thus apply to  $L \geq 5$ .

We found that  $g = 1.609 \pm 0.004$ ,  $y_i = -0.85 \pm 0.04$ , in a good agreement with a recent series result of Nickel and Rehr (Nickel *et al.*, 1990):  $y_i = -0.83 \pm 0.05$ . If we assumed a fixed value  $y_i = -0.8$ , as was done by Livet (1991), we would obtain  $K_c = 0.2216445$  (12) for the critical point. Including  $y_i$  as a variable, our final estimate of the critical point is

$$K_c = 0.221649(4).$$

If the critical point is indeed within these error bounds, Rosengren's conjecture (Rosengren, 1986)  $\tanh K_c = (\sqrt{5} - 2) \cos(\pi/8)$  or  $K_c \approx 0.2216586$  is incorrect. Our result for  $K_c$  is about three standard errors smaller than that quoted by Landau (1994), and three or more standard errors larger than values listed by Liu *et al.* (1989). A comprehensive comparison is given in the review of Landau (1994).

## 4.2 2d Ising-like models

The universal critical point ratio  $Q$  is a measure of the shape of the magnetization distribution ( $Q = \frac{1}{3}$  for a Gaussian distribution and  $Q = 1$  for the long-range ordered state). Its value for square, critical Ising systems with toroidal boundary conditions was determined by Bruce (1985), and by Burkhardt and Derrida (1985) as  $Q \approx 0.86$ .

It is a very useful quantity for accurate determination of the critical points of models that are not solvable, but can be assumed to belong to the Ising universality class. The critical point of such a model can be estimated by application of fitting procedures to Monte Carlo results for  $Q_L$  near criticality.

The ratio  $Q$  depends not only on the type of boundary conditions (Kamieniarz *et al.*, 1993a). In the isotropic case, it depends also on the aspect ratio and in the anisotropic case, on the ratio of the coupling strengths in different directions (Kamieniarz *et al.*, 1993a).

Conformal invariance has been used (Burkhardt *et al.*, 1985) to calculate  $Q$ , but unfortunately this approach is restricted to rather special boundary conditions. On the other hand, the transfer-matrix results of Burkhardt *et al.* (1985) allow a rather accurate determination of  $Q$  for square systems with toroidal boundary conditions: graphical extrapolation (Blote, Compagner and Hoogland, 1987) of the data in Table II of Burkhardt *et al.* (1985) yields  $Q = 0.856 \pm 0.002$ . For high resolution Monte Carlo simulations, however, it is desirable to find the universal ratio  $Q$  with an accuracy of more than 3 decimal places.

Considering square  $L \times L$  systems, the numerical transfer matrix estimates of  $Q_L$  ( $L \leq 17$ ) are calculated (Kamieniarz *et al.*, 1993a) and coincide with those previously published for  $L \leq 14$  (Burkhardt *et al.* 1985) up to all the decimal places quoted. Having obtained  $Q_1$ , we have extrapolated the data using, the asymptotic formula (28) for  $L \rightarrow \infty$ . We have performed direct iterative fits of this expression, taking into account different numbers of terms and we estimated

$$Q = 0.856216(1) \tag{52}$$

with a numerical uncertainty  $\pm 1$  on the last decimal place, given in parenthesis.

Finally, results for  $Q$  of some rectangular systems with different aspect ratios  $\alpha$  are shown in Table 3. For  $\alpha \leq 2$  the calculations used  $L \times 3L$  systems with  $L \leq 14$  (except for  $\alpha = 1$ , where  $L \leq 15$ ) and anisotropic couplings (Kamieniarz *et al.*, 1993a). This procedure leads to a better finite-size convergence than that using  $L \times L$  systems. As a consequence, the  $\alpha = 1$  result in Table 3 is somewhat more accurate than that in (52). For  $\alpha > 2$  the calculations used  $\alpha L \times L$  systems with  $L$  at least up to 11.

Table 3: Numerical results for the universal functions  $Q(\alpha)$  as well as for the coefficients  $a_i$  in the power series  $Q(\alpha)$ . Estimated numerical uncertainties in the last decimal place are quoted in parentheses.

| $\alpha$ | $Q(\alpha)$  | $\alpha$ | $Q(\alpha)$  | $i$ | $a_i$       |
|----------|--------------|----------|--------------|-----|-------------|
| 1.00     | 0.8562157(5) | 10       | 0.441345(1)  | 0   | 0.66965061  |
| 1.25     | 0.851947(1)  | 15       | 0.3987253(3) | 1   | 0.32377692  |
| 1.50     | 0.8415515(7) | 20       | 0.3800929(2) | 2   | -0.15701679 |
| 1.75     | 0.827049(1)  | 30       | 0.363112(8)  | 3   | -0.01878447 |
| 2.00     | 0.809678(3)  | 40       | 0.355179(6)  | 4   | 0.09094136  |
| 3.00     | 0.728090(3)  | 50       | 0.350584(5)  | 5   | -0.11922324 |
| 4.00     | 0.650069(3)  | 60       | 0.347586(4)  | 6   | 0.06618100  |
| 5.00     | 0.587126(2)  | 70       | 0.345476(3)  | 7   | 0.09431846  |
| 6.00     | 0.539396(2)  | 80       | 0.343910(3)  | 8   | -0.12230677 |
| 7.00     | 0.503811(1)  | 90       | 0.342702(2)  | 9   | -0.00847109 |
| 8.00     | 0.477176(1)  | 100      | 0.341742(1)  | 10  | 0.04733566  |
| 9.00     | 0.456964(1)  | $\infty$ | 0.333333(3)  | 11  | -0.01018046 |

Within a margin of  $3 \times 10^{-5}$ , our results for  $Q(\alpha)$  are reproduced by the expression

$$Q(\alpha) = \sum_{i=0}^{11} a_i A^i, \tag{53}$$

where  $A = 4/(\alpha + 1/\alpha) - 1$ , and the coefficients  $a_i$  are quoted in the last column of Table 3. Also, using power law fits in  $1/\alpha$  to the data for large aspect ratios, we have estimated that:

$$\lim_{\alpha \rightarrow \infty} Q(\alpha) = 0.333333(3)$$

which agrees with the value  $\frac{1}{3}$  for the Gaussian distribution describing linear systems.

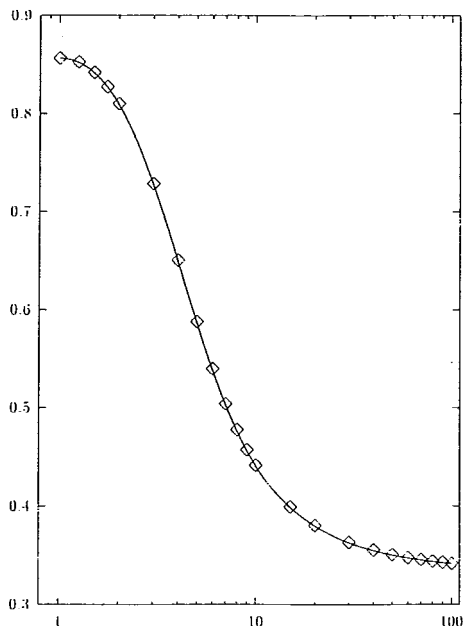


Figure 8: The universal function  $Q(\alpha)$  as a function of the aspect ratios  $\alpha$  in the extended interval  $1 \leq \alpha \leq 100$ , plotted on a semi-logarithmic scale. The curve represents fitting polynomial and interpolates through the discrete data shown by the symbol  $\diamond$ .

The critical point invariant  $Q$  is plotted in Fig. 8 on a semi-logarithmic scale versus the aspect ratio  $\alpha$ . The smooth curve represents the polynomial fitting (53).

Apart from the calculation of the ratio  $Q$  for the Ising model, we addressed the problem of the universality class for the non-interacting hard-square lattice-gas model (Baxter, Enting and Tsang, 1980). The absence or presence of a lattice-gas particle at site  $i$  is expressed by a variable  $\sigma_i = 0$  or  $\sigma_i = 1$ , respectively. Denoting the activity of the gas particles as  $z$ , the partition sum for the non-

interacting hard-square model (Baxter *et al.*, 1980) is

$$Z = \sum_{\sigma_i} z^{\sum_i \sigma_i} \prod_{\langle i,j \rangle} (1 - \sigma_i \sigma_j) \quad (54)$$

where the product is over all pairs of nearest-neighbour sites, and guarantees that configurations with interpenetrating particles do not contribute to  $Z$ .

In absence of an exact solution, Baxter *et al.* (1980) applied series expansion techniques to determine the critical exponents of this model. They found that the specific heat exponent  $\alpha' = 0.09 \pm 0.05$  which was different from the exactly known value of the two-dimensional Ising model  $\alpha = 0$ . Subsequent analyses of the finite-size scaling behaviour of the temperature derivative of the correlation length (Wood and Goldfinch, 1980; Racz, 1980) did not show significant deviations from the Ising universality. However, we found the result by Baxter *et al.* (1980) sufficiently challenging to find more compelling numerical evidence that the hard-square model is inside the Ising universality class.

On the basis of the result for the critical activity (Blöte and Wu, 1990)

$$z_c = 3.796255174(3),$$

where the translational symmetry of the model (54) is spontaneously broken, the series expansions evaluated by Baxter *et al.* (1980) can be reanalysed.

Thus we consider (Kamieniarz and Blöte, 1993b) an expansion of the order parameter (*i.e.* the staggered density)  $R$  in terms of the high-density parameter  $x = 1/z$ . From the ratio analysis of  $R \sim^s(x)$ , using  $z_c$  and the coefficients listed in Table II of Baxter *et al.* (1980) we have estimated that the critical exponent  $\beta = 0.1249(1)$ , in agreement with Ising universality.

The subsequent Dlog Padé analysis of the series  $R(x)$  (as that in Table I of Baxter *et al.* (1980)) and the smooth dependence (Fig. 9) of the residues of  $\frac{d}{dx} \ln R(x)$  on the distance of the corresponding poles from the critical value  $x_c = 0.263417488$  indicate that  $\beta$  does not differ from  $1/8$  by more than a few times  $10^{-5}$ .

To calculate  $\alpha$ , the second derivative  $\rho^{(2)} \equiv \frac{d^2}{dx^2} \rho'$  of the lattice-gas density series  $\rho'$  is chosen which is more singular than  $\rho$  and can be found from the series  $\rho' = 1 - 2\rho = \sum_{n=1}^{\infty} \rho_n x^n$ , where the coefficients  $\rho_n$  are determined by those given in Appendix B of Baxter *et al.* (1980). Performing the Dlog analysis of the  $\rho^{(2)}$  series (Kamieniarz *et al.*, 1993b), we estimate  $\alpha' = -0.1(1)$  which indicates that  $\alpha'$  may be smaller than the result obtained by Baxter *et al.* (1980) from the  $R(\rho')$  series. The dependence of the  $\alpha'$  estimates on the distance from the critical point  $x_c$  is shown in Fig. 10.

In Tables 4 and 5 our additional differential approximant analyses (Fisher and Au-Yang, 1979) of  $iT^1(\rho')$  and  $\rho(x)$  series are shown. The columns denoted

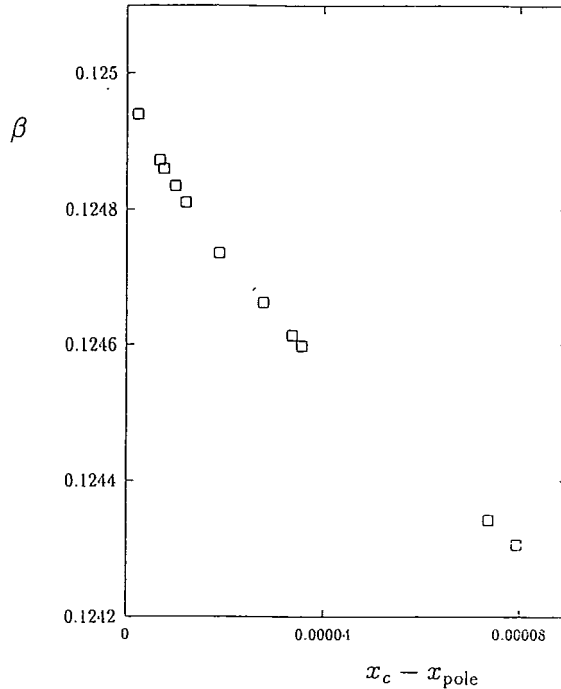


Figure 9: The residues of the D-log Pade approximants of the series  $R(x)$  versus the deviations of the corresponding poles from the critical value  $x_c$

$N, L, M$  display the degrees of the corresponding polynomials.  $\overline{\rho}'_c$  and  $\overline{x}_c$  represent the calculated unbiased critical parameters  $\rho'_c$  and  $x_c$  which are obtained from the given approximants. Subscripts  $u$  and  $b$  denote the unbiased and biased (choosing  $\rho'_c = 0.264514$ ,  $x_c = 0.2634175$ ) estimates of the corresponding critical exponents. The accuracy of the  $u$ -exponents depends strongly on the accuracy of the estimates  $\overline{\rho}'_c$  and  $\overline{x}_c$ . However, the  $b$ -exponents deviate from the Ising values within a margin of 0.002 and 0.005 for  $\beta/(1 - \alpha')$  and  $\alpha'$ , respectively (where we disregard the estimate for the approximant [6,5,10]).

In addition, we consider the lattice-gas model (54) on  $L \times L$  and  $L \times \infty$  square lattices with periodic boundary conditions. To enable the introduction of two sublattices in a checkerboard-like fashion,  $L$  is restricted to be even. We use the transfer matrix technique (Kamieniarz *et al.*, 1993b) in order to calculate the partition sum (54), as well as some of its derivatives.

A finite-size analysis is used to determine  $y_h$  and  $y_t$ . Other exponents follow from these by means of scaling. Here, the main interest is in the value of  $y_t$  in view of its relevance for  $\nu = 2 - d/y_t$ . The assumptions

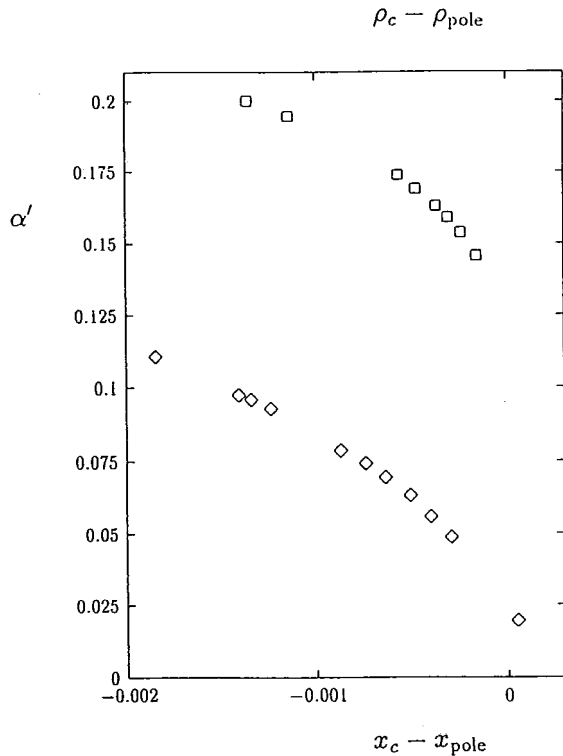


Figure 10: The dependence of the  $\alpha'$  estimates found from the D-log Padé approximants on the deviations of the poles from the critical point. The present data are shown versus  $x_c - x_{pole}$  by  $\diamond$ , and those of Baxter *et al.* versus  $\rho_c - \rho_{pole}$  by  $\square$ .

involved amount to the analyticity of renormalisation transformations employing an additional finite-size field (Barber, 1983)  $1/L$  with exponent  $y_L = 1$ .

We have determined finite-size data for several quantities: the density  $\rho_L$  of the lattice gas particles, the specific heat  $c_L$ , the staggered susceptibility  $\chi_L$ , and the temperature derivative  $g'_i(L)$  of the inverse magnetic correlation length. They are expected (Kamieniarz *et al.*, 1993b) to fulfil the finite-size scaling relations

$$\rho_L \simeq \rho_c + L^{y_t-d}(a_1 + a_2 L^{-p}), \quad c_L \simeq L^{2y_t-d}(b_1 + b_2 L^{-q}),$$

$$\chi_L \simeq L^{2y_h-d}(c_1 + c_2 L^{-r}), \quad g'_i(L) \simeq L^{y_t-1}(d_1 + d_2 L^{-w}),$$

where  $d = 2$  is the dimensionality and the terms with exponents  $p, r, q, w$  represent corrections to scaling. As an example, we show the results for a square system in Table 6. The scaling behaviour of all these data is in an accurate agreement (Kamieniarz *et al.*, 1993b) with Ising universal exponents.

Another approach intimately related with renormalisation was made using the hypothesis of conformal invariance (Cardy, 1987). The temperature and

Table 4: The differential approximant analysis of the series  $R^{-1}(\rho')$ .

| N | L | M  | $\bar{\rho}'_c$ | $(\frac{\beta}{1-\alpha'})_u$ | $(\frac{\beta}{1-\alpha'})_b$ |
|---|---|----|-----------------|-------------------------------|-------------------------------|
| 7 | 7 | 7  | 0.264465        | 0.118388                      | 0.126657                      |
| 8 | 5 | 8  | 0.264488        | 0.122358                      | 0.126509                      |
| 7 | 6 | 8  | 0.264483        | 0.121542                      | 0.126559                      |
| 8 | 4 | 9  | 0.264535        | 0.129885                      | 0.126066                      |
| 6 | 7 | 8  | 0.263892        | 0.018301                      | 0.126448                      |
| 7 | 5 | 9  | 0.264491        | 0.122845                      | 0.126751                      |
| 5 | 8 | 8  | 0.264692        | 0.157027                      | 0.125629                      |
| 6 | 6 | 9  | 0.264552        | 0.132852                      | 0.126476                      |
| 5 | 7 | 9  | 0.264583        | 0.137947                      | 0.126610                      |
| 6 | 5 | 10 | 0.264471        | 0.119259                      | 0.145598                      |
| 4 | 8 | 9  | 0.264060        | 0.041619                      | 0.123054                      |
| 5 | 6 | 10 | 0.264597        | 0.140181                      | 0.124088                      |

magnetic exponents were determined using the relation (29) between exponents and the finite-size amplitude of the associated correlation lengths for the infinite strips. The ensuing results (Kamieniarz *et al.*, 1993b)

$$y_t = 1.000000(1), \quad y_h = 1.875000(1)$$

are in precise agreement with the exactly known Ising values  $y_h = 15/8$  and  $y_t = 1$ .

In addition to these results for the exponents, we have also found the critical density

$$2 \times p_c = 0.73548600(1)$$

and the universal critical point ratio (Kamieniarz *et al.*, 1993a)

$$Q = \langle R^2 \rangle^2 / \langle R^4 \rangle = 0.85625(5),$$

the latter in agreement with the corresponding Ising value (52) for ferromagnetic Ising models with periodic boundaries of the square symmetry.

### 4.3 Quasi one-dimensional magnets

Quasi-one-dimensional magnets have attracted a great deal of interest due to nonlinear spin dynamic effects and the recognition of the role of the spin value in the ground state critical properties. An extensive account of the theoretical and experimental results can be found elsewhere (Mikeska and Steiner, 1991; Halperin, 1992).

Table 5: The differential approximant analysis of the series  $\rho(x)$ .

| N | L | M  | $\bar{x}_c$ | $(1 - \alpha')_a$ | $(1 - \alpha')_b$ |
|---|---|----|-------------|-------------------|-------------------|
| 7 | 6 | 7  | 0.263490    | 0.985605          | 0.999678          |
| 8 | 4 | 8  | 0.263516    | 0.981007          | 0.994742          |
| 6 | 7 | 7  | 0.263417    | 0.999936          | 0.999765          |
| 7 | 5 | 8  | 0.263608    | 0.963034          | 0.998233          |
| 6 | 6 | 8  | 0.263422    | 0.998815          | 0.999693          |
| 7 | 4 | 9  | 0.263491    | 0.984604          | 0.995466          |
| 5 | 7 | 8  | 0.263417    | 0.999779          | 0.999766          |
| 6 | 5 | 9  | 0.263549    | 0.973867          | 0.100050          |
| 4 | 8 | 8  | 0.263415    | 0.999955          | 0.999424          |
| 5 | 6 | 9  | 0.263494    | 0.984681          | 0.999637          |
| 4 | 7 | 9  | 0.263330    | 1.017277          | 1.000238          |
| 5 | 5 | 10 | 0.263543    | 0.975050          | 0.995529          |

First, we recall here the zero-field specific heat results for *CHAB* (i.e. the spin  $S = 1/2$  compound  $C_6H_{11}NH_3CuBr_3$ ). In Fig. 11 the dashed curve represents the experimental data, whereas our numerical estimates (Campana *et al.*, 1990) are given by solid circles. The vertical intercepts show the numerical uncertainties for  $N \leq 12$  in our extrapolation procedure (34).

In Fig. 12 the *CHAB* high-field specific-heat data are depicted. The small symbols denoted by crosses and open and solid circles show the experimental excess specific heat  $\Delta C(T,B)$ . The bigger crosses and solid circles with the error bars represent our estimates found from the polynomial fitting (32). We

Table 6: The finite-size data  $2\rho_L$ ,  $c_L$  and  $\chi_L$  calculated numerically for square systems.

| L  | $2\rho_L$          | $c_L$              | $\chi_L$          |
|----|--------------------|--------------------|-------------------|
| 2  | 0.8090898056421140 | 0.1402349991566989 | 0.724743813172343 |
| 4  | 0.7749712801688777 | 0.1922474459514767 | 2.447647203710980 |
| 6  | 0.7616725216302425 | 0.2246002865877822 | 4.978297322277479 |
| 8  | 0.7550639427551426 | 0.2477057485415912 | 8.241664994051973 |
| 10 | 0.7511214217544006 | 0.2656570381718074 | 12.18609189883877 |
| 12 | 0.7485021560614531 | 0.2803252992432338 | 16.77381425559746 |
| 14 | 0.7466353591805462 | 0.2927219631820310 | 21.97568172323616 |
| 16 | 0.7452373256688473 | 0.3034545757008545 | 27.76817664548804 |

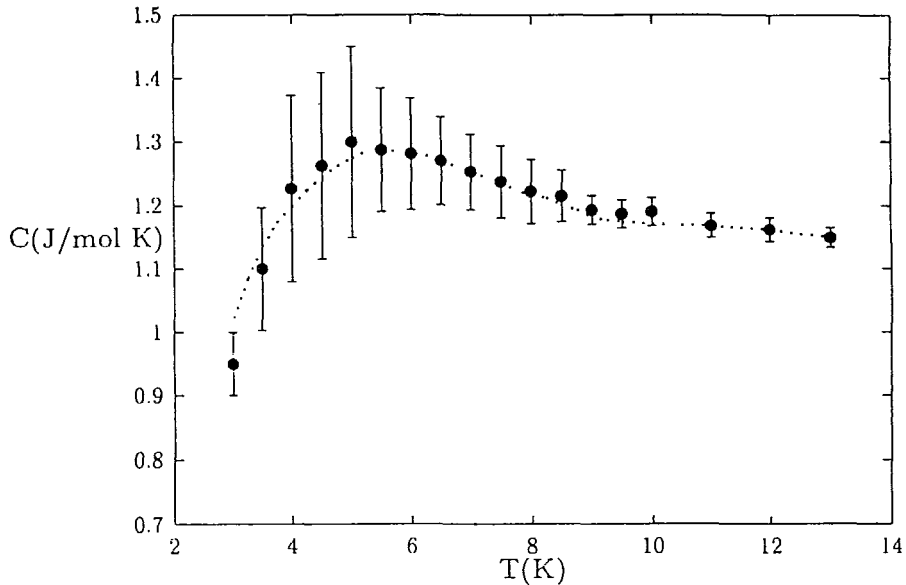


Figure 11: Zero-field specific heat of CHAB. The dashed curve represents the experimental results. Present theoretical results are shown by solid circles with error bars.

encountered a good convergence of the extrapolations for temperatures  $T \geq 10\text{K}$ , including the position of the peak for  $B = 3\text{T}$  and we found agreement with *QTM* predictions (Kopinga *et al.*, 1990).

The zero-field specific heat is also calculated for  $C_6H_{11}NH_3CuCl_3$  (the  $S = \frac{1}{2}$  compound abbreviated as *CHAC*) and is shown in Fig. 13. From the ferromagnetic resonance experiment it has been established that *CHAC* can be described by the anisotropic Heisenberg Hamiltonian with  $J_x/k_B = 45.52\text{K}$ ,  $J_y/k_B = 44.99\text{K}$  and  $J_z/k_B = 44.49\text{K}$ . In Fig. 13 the experimental curve is drawn in the solid line with a sharp peak corresponding to the phase transition point to the three-dimensional (3D) ordering. Our results are marked by the circles and are consistent with the experimental findings down to  $2\text{K}$  above the transition temperature. An additional fitting procedure for *CHAC* was carried out by Kopinga, Delica, Leschke and Riedel (1993).

A considerable amount of experiments has been performed (Mikeska *et al.*, 1991) on  $CsNiF_3$ , the spin  $S = 1$  quasi-one-dimensional ferromagnet. The microscopic parameters

$$J/k_B = 23.6\text{K}, \quad A/k_B = 9\text{K}, \quad g = 2.4 \quad (55)$$

of the Hamiltonian describing  $CsNiF_3$  were first determined (Steiner, Villain and Windsor, 1976) by fitting the observed energy spectra to the theoretical magnon

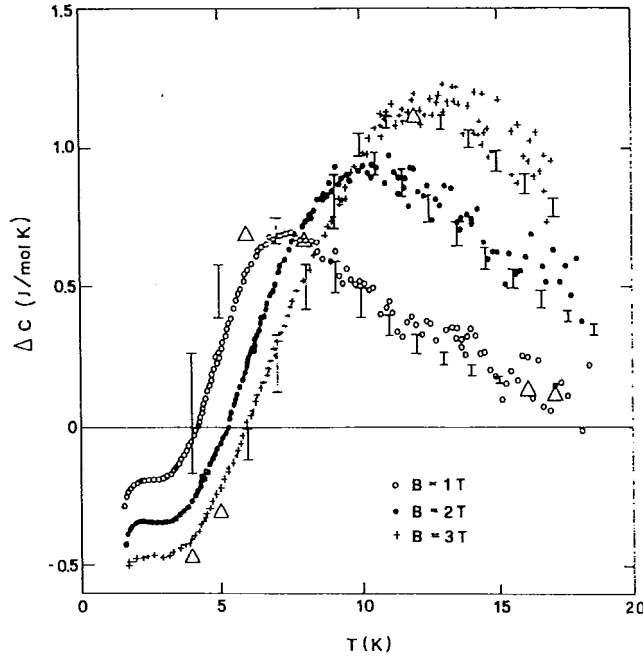


Figure 12: Excess specific heat  $\Delta C(T, B) = C(T, B) - C(T, 0)$  of CHAB for  $B = 1, 2,$  and  $3 T$ . Open circles, solid circles, and small crosses represent the experimental data. Bigger crosses and points with error bars illustrate present estimates.

dispersion relation. Due to the discrepancies between the theoretical predictions and the observed static properties evidenced in numerical calculations, new fitting procedures were carried out by Delica, de Jonge, Kopinga, Leschke and Mikeska (1991) and Campana *et al.* (1992a) which led to the following sets of the parameters

$$J/k_B = 25K, \quad A/k_B = 7.7K, \quad g = 2.1 \quad (56)$$

and

$$J/k_B = 20.5K, \quad A/k_B = 8.71K, \quad g_{\parallel} = 2.23, \quad g_{\perp} = 2.28 \quad (57)$$

respectively. In both numerical procedures the values of  $g$  were fixed and only  $J$  and  $A$  were subject to variation.

We found the competing predictions (55), (56), (57) together with a new *SCHA* approach (Cuccoli, Tognetti, Verrucchi and Vaia, 1992) challenging enough to start new large-scale simulations (Campana *et al.*, 1996) by recourse to the finite-size and *QTM* calculations. As the sets (55), (56), (57) were found from different fitting procedures and no significant experimental results have been

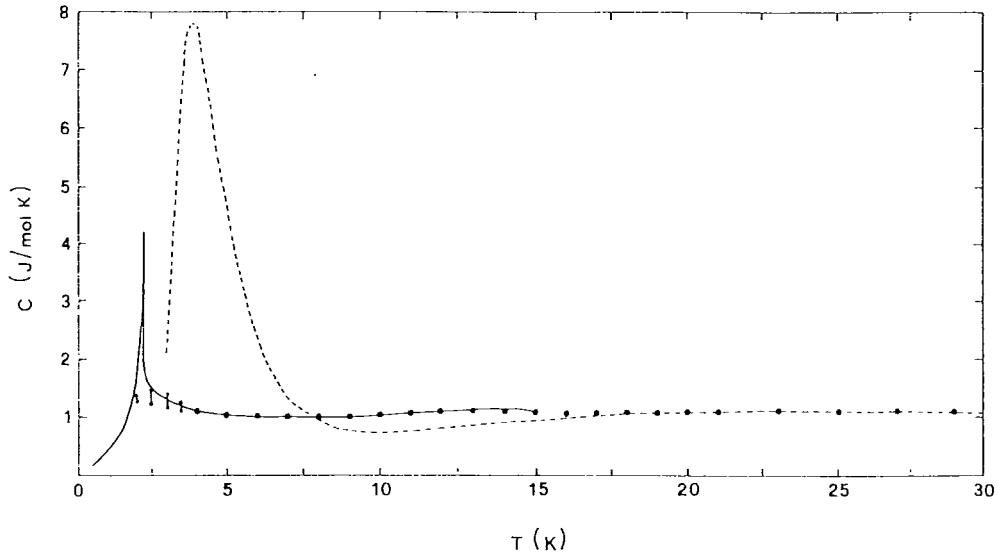


Figure 13: Zero-field specific heat of *CHAC*. The experimental data are plotted by the continuous line and our estimates are displayed by the symbols.

reported (to our knowledge) in the meantime, so that we compared the predictions following from these values of the parameters and we determined within the unique technique the optimum set (57) with respect to static properties of *CsNiF<sub>3</sub>*.

We start presentation of our new results (Campana *et al.*, 1996) from the zero-field longitudinal susceptibility  $\chi_{||}$ . This quantity displays a maximum in low temperatures which is sensitive to the choice of parameters. Our numerical data are given in Fig. 14 for sets (57), (56), (55), respectively and the results of measurements (Dupas and Renard, 1977) are depicted by full circles. For set (57) found in (Campana *et al.*, 1992a), the agreement is excellent whereas some deviations of the order of 5-6% occur (Fig. 15) near the maximum if set (56) is used. Well pronounced discrepancy between experiment and simulations for set (55) appears in the entire temperature region.

The zero-field perpendicular susceptibility  $\chi_{\perp}$  data are shown in Fig. 15 - 16 for the same parameters as before and using the same symbols as in Fig. 14. In addition, dotted curve in Fig. 16 illustrates the predictions of Cuccoli *et al.* (1992) The results of our simulations for  $\chi_{\perp}$  show systematic deviations with respect to the experimental data, of the order of 2%, irrespective of the parameter values. The values (56), (57) lead to an underestimation, whereas those in (55), to an overestimation. We also note that the theoretical *SCHA*

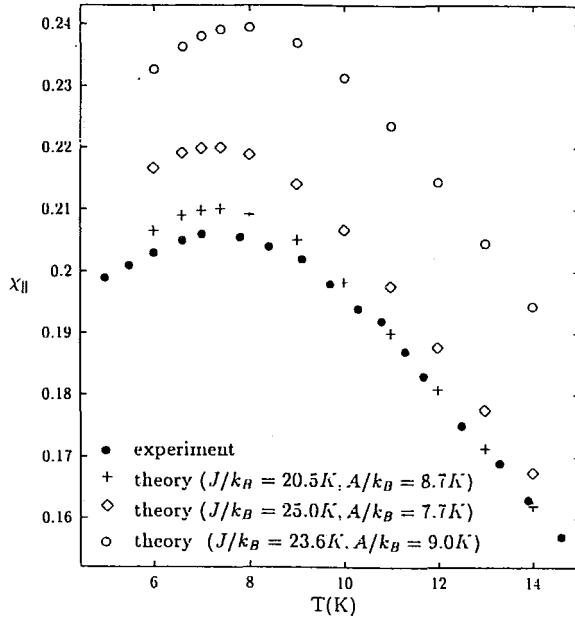


Figure 14: The temperature dependence of  $\chi_{||}$  in molar units. The symbols and the parameters are specified in the label.

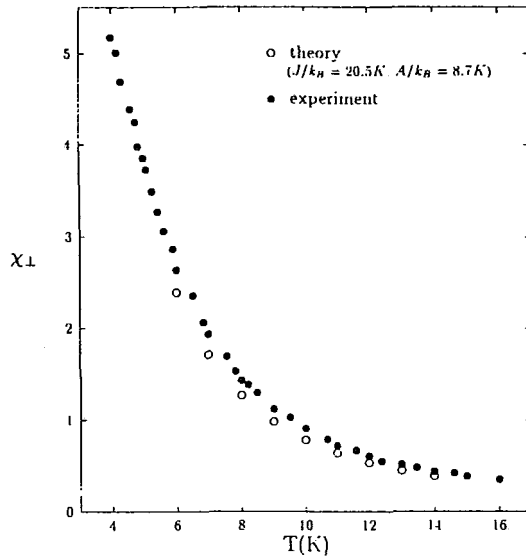


Figure 15: The temperature dependence of the molar  $\chi_{\perp}$ . The symbols  $\bullet$  and  $\circ$  represent the experimental and numerical data, respectively.

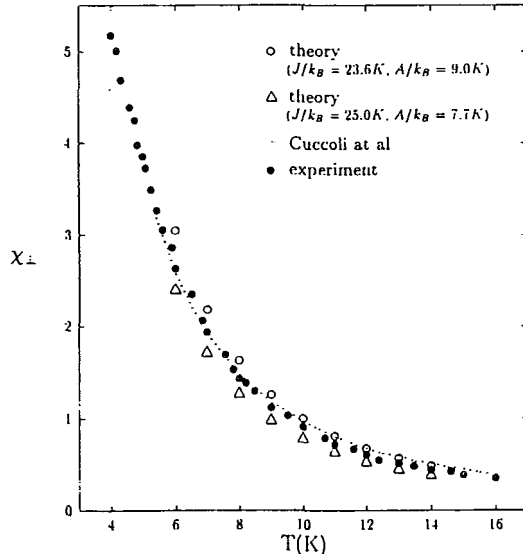


Figure 16: The temperature dependence of the molar  $\chi_{\perp}$ . Notation as in Fig. 15.

curve in Fig. 16 does not coincide with our predictions within the error of our simulations.

In Fig. 17 we present the excess specific-heat data in the field 5 kGs. The corresponding experimental data (Ramirez and Wolf, 1985) are shown by full circles and our results by  $\diamond$ ,  $\square$ ,  $\triangle$  symbols for parameter (55), (56), (57), respectively. We also plot by the dotted curves the theoretical *SCHA* predictions as reported in (Cuccoli *et al.*, 1992). Our findings for the excess specific-heat nearly coincide for parameters (56) and (57). We do not confirm the quantitative agreement with experiment for parameters (55), although the deviations between our results and those of *SCHA* do not exceed 20%.

In conclusion, the best agreement with static properties of  $CsNiF_3$  is reached for the parameter set (57).

For the antiferromagnetic Haldane-gap system  $CsNiCl_3$ , it has been established from susceptibility and specific heat measurements (de Jongh and Miedema, 1974; Moses, Ehrenfreud, Makovsky and Shechter, 1977) that  $-J/k_B = 26 - 27$  K. However, neutron-scattering experiments (Morra, Armstrong, Buyers and Hirakawa, 1988), performed in order to test the Haldane conjecture, have led to a somewhat higher value  $J/k_B = -33.2$  K.

From our finite-size calculations (Campana, Caramico D'Auria, Esposito, Esposito and Kamieniarz, 1992b) we found the following set of parameters:

$$J/k_B = -27 \pm 3 \text{ K}, \quad D/J = 0.05, \quad g = 2.23, \quad (58)$$

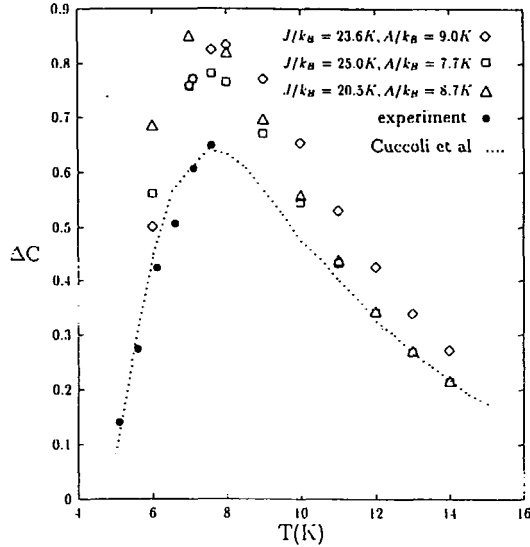


Figure 17: The temperature dependence of the excess specific heat in molar units in the applied field  $B = 5$  kGs. The experimental data are given by the full circles. The numerical data for different parameters are presented by the symbols explained in the labels. The SCHA predictions are plotted by the dotted curve.

giving the best fit to the static measurements. These values confirm the previous findings from the static measurements (de Jongh *et al.*, 1974; Moses *et al.*, 1977). In particular, our  $g$  value agrees very well with the one found from the ESR experiment (Achiwa, 1969). The slight anisotropy in the experimental susceptibility data can be accounted for by a small anisotropy in  $g$ .

The numerical results (Campana *et al.*, 1992b) for the zero-field specific heat of  $CsNiCl_3$  are represented in Fig. 18 as the solid line, whereas the dotted line gives the numerical results for  $J/k_B = -33.2$  K. The corresponding experimental data are represented by the circles.

In Fig. 19 we plot our numerical predictions for the parallel susceptibility  $\chi_{||}$  (to avoid an overlap, we skip our estimates for  $\chi_{\perp}$ ). The symbols represent the experimental data: the open circles refer to  $\chi_{||}$  and the triangles to  $\chi_{\perp}$ . The dashed curve represents our results for  $\chi_{||}$ , using the value  $J/k_B = -33.2$  K, which underestimate the experimental data and deviate well above the uncertainties in our extrapolations, denoted by the vertical error bars. These findings have been confirmed by our recent *QTM* calculations (Kamieniarz *et al.*, 1996a).

The Haldane-gap systems attract a lot of interest (Halperin, 1992; Ramirez, Cheong and Kaplan, 1994) and new antiferromagnetic  $S = 1$  chains are synthesized (Gadet, Verdagner, Briois, Glezis, Renard, Beauoillain, Chappert, Goto,

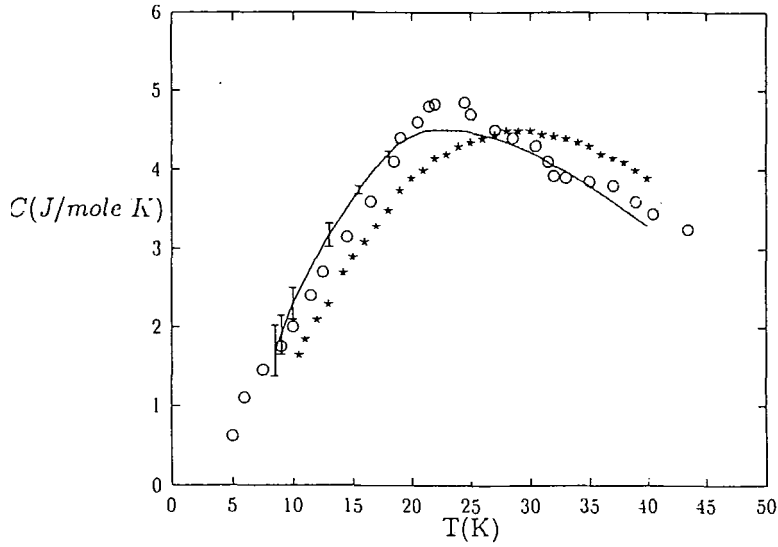


Figure 18: Specific heat of  $\text{CsNiCl}_3$ . The open circles refer to experimental data. The finite-chain results for  $J/k_B = -27 \text{ K}$  and  $D/J = 0.05$  are drawn by the solid line with error bars. The dotted line refers to  $J/k_B = -33.2 \text{ K}$ .

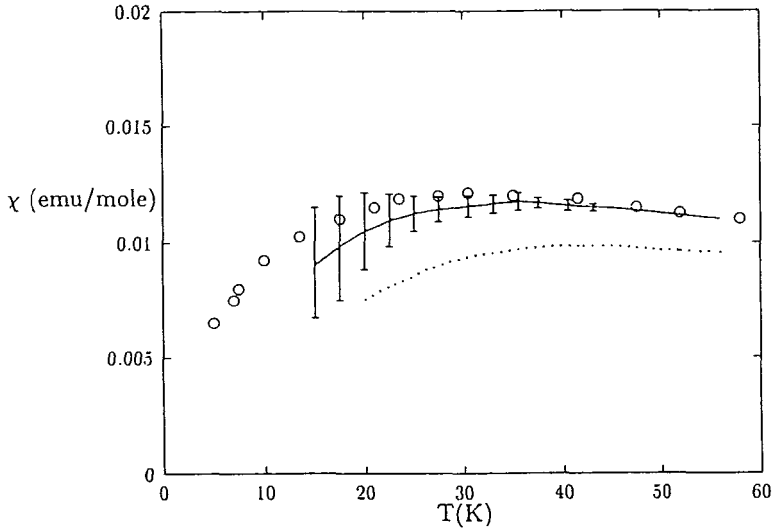


Figure 19: Susceptibility of  $\text{CsNiCl}_3$ . Solid line: numerical data for  $J/k_B = -27 \text{ K}$  and  $D/J = 0.05$ . Dashed line: our data for  $J/k_B = -33.2 \text{ K}$ . Errors bars are shown by the intercepts. The symbols report the experimental data: the circles  $\chi_{\parallel}$  and the triangles  $\chi_{\perp}$ .

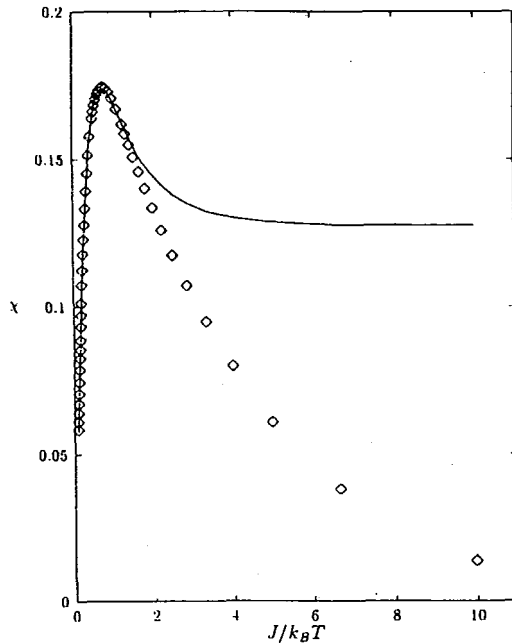


Figure 20: The temperature dependence of the isotropic susceptibility for the  $S = 1$  antiferromagnetic Heisenberg chain. The symbols illustrate the numerical data and the curve represents the high-temperature expansion results.

Le Dang and Veillet, 1991; Darriet and Regnault, 1993). To help interpret the susceptibility measurements we calculated within *QTM* (Kamieniarz *et al.*, 1996a) the temperature dependence of the susceptibility in the isotropic limit. Our results are shown in Fig. 20 by the  $\diamond$  symbols. So far only high-temperature series expansion results of Weng (Weng, 1968) have been available and commonly used. The latter are drawn by the continuous line in Fig. 20.

#### 4.4 Spin-dynamics for the classical anisotropic chain

Following Gerling *et al.* (1990), we have interpreted results of our simulations for the  $x$  and  $y$  polarizations of the neutron scattering laws for  $CsNiF_3$  by recourse to the sine-Gordon theory (Allroth and Mikeska, 1981). The sine-Gordon theory restricts spins to the XY-plane, but on general grounds (Kakurai, Steiner and Dorner, 1990) we expect to see out-of-plane fluctuations which at least give rise to a single spin-wave peak  $S_z^{sw}(q, \omega)$  with the Lorentzian line shape adopted.

We considered (Grille *et al.*, 1992) the spins as three-dimensional vectors of

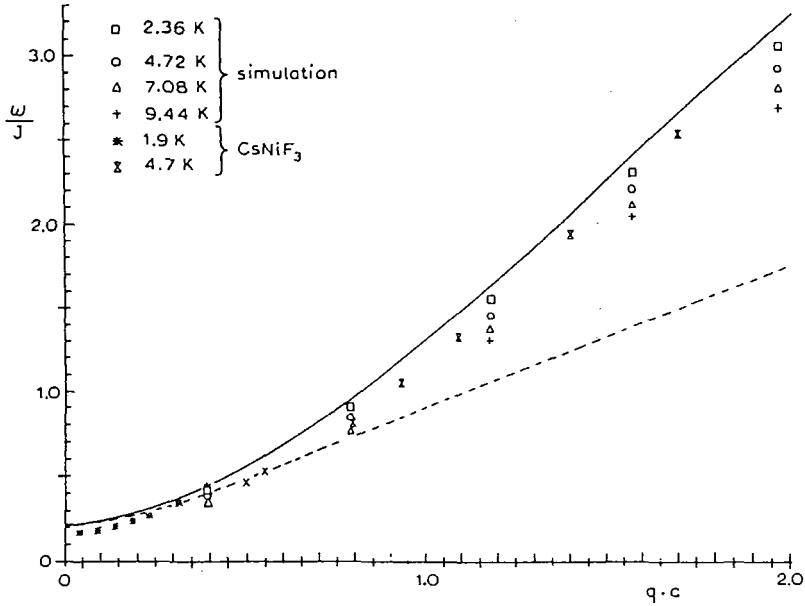


Figure 21: The spin-wave dispersion  $\omega(q)$ . The temperatures for the simulation results (the magnetic field  $B = 1$  T and the anisotropy  $A/k_B = 9.0$  K) and the experimental results are given in the label. A harmonic approximation and the sine-Gordon result are plotted by the solid line and the dashed line, respectively.

unit length and we chose

$$J/k_B = 23.6K, A/k_B = 9.0K \text{ or } A/k_B = 4.5K, g = 2.25$$

Typically, the neutron scattering laws found here are similar to those for the XY model (Gerling *et al.*, 1990), although the interpretation is more difficult and not always unique.  $S_z(q, \omega)$  consists of a single narrow spin-wave peak, whereas  $S_x(q, \omega)$  and  $S_y(q, \omega)$  develop a double-peak structure.

The fitting procedure, similar to that of Gerling *et al.* (1990), leads to the following predictions (Grille *et al.*, 1992). There exist out-of-plane fluctuations yielding well-defined spin-wave excitations. The spin-wave dispersion found from  $S_y(q, \omega)$  is presented in Fig. 21 for  $A/k_B = 9$  K and  $B = 1$  T. Our results are reported by the symbols defined in Fig. 21. The experimental data, reported by asterisks, are taken after Steiner, Kakurai and Kjems (1983) in the region  $qa \leq 0.4$  whereas for  $qa \geq 0.4$  we have interpolated the results of Steiner and Kjems (1977). The continuous curve is a harmonic approximation and the dashed line is the result of the sine-Gordon model. For low temperatures and small wave

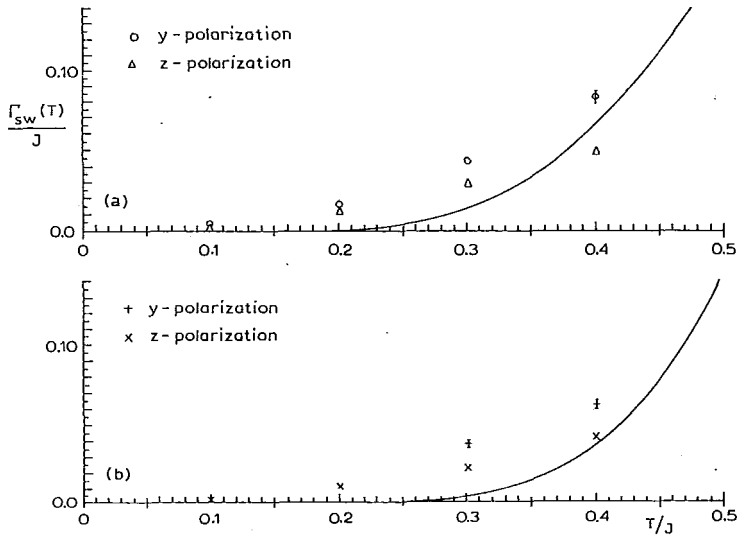


Figure 22: The  $q$ -dependence of the spin-wave line widths  $\Gamma_{sw}$ . The temperatures are as indicated and the magnetic field  $B = 1 T$  and the anisotropy  $A/k_B = 9.0 K$ .

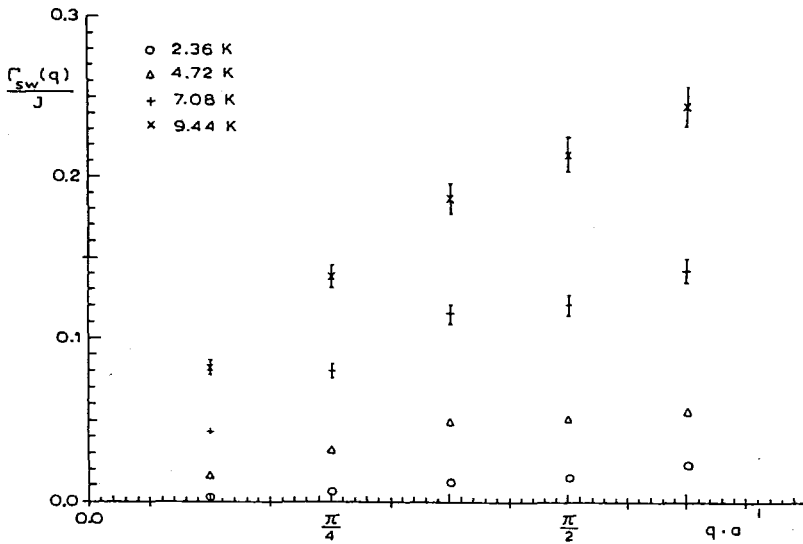


Figure 23: The  $T$ -dependence of the spin-wave halfwidths  $\Gamma_{sw}$ . The polarization is as indicated, the anisotropy  $A/k_B = 9.0 K$ , and the wave vector  $qa = \pi/8$ . The magnetic field  $B = 1 T$  (a) and  $B = 2 T$  (b). The lines show the corresponding sine-Gordon predictions.

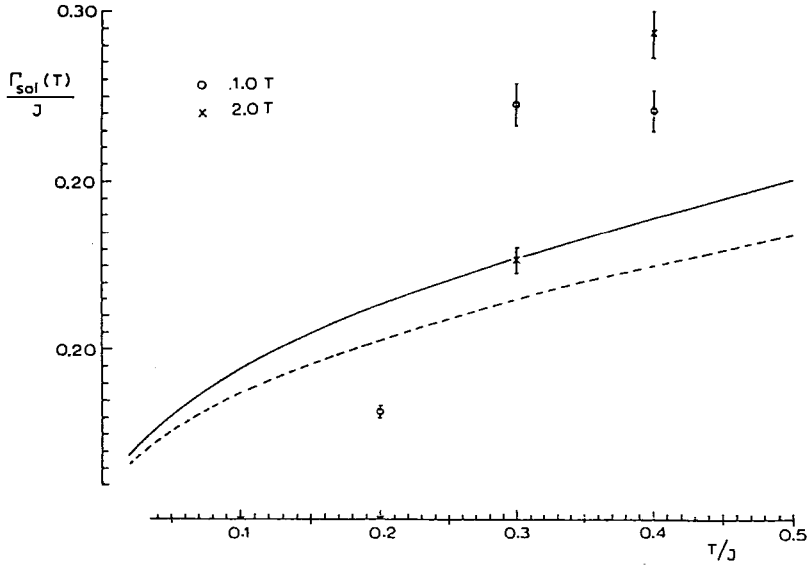


Figure 24: The  $T$ -dependence of the soliton halfwidths  $\Gamma_{sol}$ . The anisotropy  $A/k_B = 9.0 K$ , and the wave vector  $qa = \pi/8$ . The magnetic field is as indicated. The solid and dashed lines show the sine-Gordon predictions for  $B = 1 T$  and  $B = 2 T$ , respectively.

vectors  $q$  the agreement between the sine-Gordon theory, the computer simulations and the experiments is quite good. However, the dispersion is thermally renormalised. For  $T = 4.7 K$  this renormalisation is of the order of 8 — 10%. This effect has usually been neglected (Kakurai *et al.*, 1990; Steiner *et al.*, 1977).

In view of the interesting narrowing of zero-field in-plane spin-wave linewidths observed experimentally (Kakurai *et al.*, 1990) at 4.7 K, we present similar results for  $B = 1 T$  in Fig. 22. We find that in the presence of the magnetic field the narrowing cannot be observed as clearly as in experiments. The corresponding  $T$ -dependence of the  $y$ - and  $z$ -polarization linewidths is displayed in Fig. 23. Finally, in Fig. 24 we show the  $T$ -dependence of the widths of the central peaks for the  $y$ -polarization.

The half widths of this soliton peak reveal serious disagreement with the sine-Gordon predictions depicted by the solid and dashed lines for 1 and 2 T, respectively. Our data points show qualitatively different behaviour with respect to the sine-Gordon results. We attribute these deviations to the strong out-of-plane fluctuations. However, in low temperatures the sine-Gordon theory is a reasonable starting point for the analysis of experimental results. For higher temperatures the out-of-plane fluctuations must be included in the theory.

## 5 Conclusions

In the area of phase transitions the precision of our simulation results reached the sixth decimal place. It was possible due to careful selection of simulation algorithms, good statistics of the Monte Carlo data and the use of a perturbative transfer matrix approach, yielding directly the magnetization moments. Important was also the combination of different geometries, the asymptotic finite-size scaling analysis and implementation of conformal invariance.

High precision was also reached in the field of quantum spin chains down to low temperatures. Here the combination of the *QTM* methods together with the direct finite-size diagonalization technique has been used. Large systems (e.g.  $200 \times 14$  for  $S = 1$ ) were simulated and careful numerical analysis was applied.

Some unresolved issues in the universal classification of phase transitions in the framework of conformal field theory (Klümper and Pearce, 1993) and new challenging experiments on mesoscopic magnetic particles (Gatteschi, Caneschi, Pardi and Sessoli, 1994) considerably justify further effort in simulation of the low-dimensional magnets.

The spin dynamics study of the classical Heisenberg ferromagnet is only touched here in relation to the easy-plane chains modelling  $CsNiF_3$ . However, the method is suitable for the dynamic study in higher dimensions (Landau, 1994) and in other systems.

## Acknowledgements

The author is grateful to H. Blöte, L.S. Campana, A. Caramico D'Auria, R. Dekeyser, F. Esposito, U. Esposito, F. Mallezie, G. Musial and P. Pawlicki for their contribution to various parts of the research reviewed here.

The support from the Committee for Scientific Research via grant No. 8 T11F 015 09 is also acknowledged. A part of numerical calculations was performed in the Supercomputing and Networking Center in Poznań.

## References

- Achiwa, N. (1969) Linear antiferromagnetic chains in hexagonal ABC13-type compounds (A; Cs or Rb, B; Cu, Ni, Co or Fe). *J. Phys. Soc. Jpn.*, **27**, 561
- Aharony, A. and M.E. Fisher (1983) Nonlinear scaling fields and corrections to scaling near criticality. *Phys. Rev.*, **B27**, 4394
- Allroth, E. and H.J. Mikeska (1981) Solitons and magnons in sine-Gordon like magnets. *Z. Phys.*, **B43**, 209

- Baillie, C.F., R. Gupta, K.A. Hawick and G.S. Pawley (1992) Monte Carlo renormalization group studies of the three-dimensional Ising model. *Phys. Rev.*, **B45**, 10438
- Barber, M.N. (1983) Finite-Size Scaling. In C. Domb and J.L. Lebowitz (Eds.), *Phase Transitions and Critical Phenomena*, Vol.8, Academic Press, London
- Baxter, R.J. (1982) Exactly Solvable Models in Statistical Mechanics. Academic Press, New York
- Baxter R.J., I.G. Enting and S.K. Tsang (1980) Hard-square lattice gas. *J. Stat. Phys.*, **22**, 465
- Binder, K. (1981) Finite size scaling analysis of Ising model block distribution functions. *Z. Phys.*, **B43**, 119
- Blöte, H. (1975) The specific heat of magnetic linear chains. *Physica*, **B79**, 427
- Blöte, H., A. Compagner and A. Hoogland (1987) The simple quadratic Ising model with crossing bonds. *Physica*, **A141**, 375
- Blöte, H. and G. Kamieniarz (1993) Finite-size calculations of the three-dimensional Ising model. *Physica*, **A196**, 455
- Blöte, H. and G. Kamieniarz (1994) Simulations of the 3D Ising model at criticality. *Acta Phys. Polon.*, **A85**, 389
- Blöte, H. and X.N. Wu (1990) Accurate determination of the critical line of the square Ising antiferromagnet in a field. *J. Phys. A: Math. Gen.*, **23**, L627
- Bonner, J.C. and M.E. Fisher (1964) Linear magnetic chains with anisotropic coupling. *Phys. Rev.*, **A135**, 640
- Bruce, A.D. (1985) Universality in the two-dimensional continuous spin model. *J. Phys. A: Math. Gen.*, **18**, L873
- Burkhardt, T.W. and B. Derrida (1985) Moments of the total magnetization and conformal invariance in the finite two-dimensional Ising model. *Phys. Rev.*, **B32**, 7273
- Cachine, J., J.R. Drugovich de Feli and N. Caticha (1989) Non-universal exponents and marginal operators via a Monte Carlo renormalisation-group. *J. Phys. A: Math. Gen.*, **22**, 1639
- R. Dekeyser, *Phys. Rev.* **B42**, 10765 (1990)
- Campana, L.S., A. Caramico D'Auria, U. Esposito, G. Kamieniarz and R. Dekeyser (1990) Specific heat of  $(\text{C}_6\text{H}_{11}\text{NH}_3)\text{CuBr}_3$  and  $(\text{C}_3\text{H}_7\text{NH}_3)\text{CuCl}_3$  within series analysis of finite chain data. *Phys. Rev.*, **B42**, 10765
- Campana, L.S., A. Caramico D'Auria, F. Esposito, U. Esposito, R.W. Gerling, and G. Kamieniarz (1992a) Static properties of quantum spin  $S=1$  chains: TMNB, TMNC and  $\text{CsNiF}_3$ . *J. Phys.: Cond. Matter*, **4**, 2915
- Campana L.S., A. Caramico D'Auria, F. Esposito, U. Esposito, G. Kamieniarz (1992b) Finite-Chain approach to the study of  $\text{CsNiCl}_2$ . *Phys. Rev.*, **B45**, 5035

- Campana, L.S., A. Caramico D'Auria, F. Esposito, U. Esposito and G. Kamieniarz (1996), *Phys. Rev.* **B**
- Cardy, J.L. (1987) Conformal Invariance. In C. Domb and J.L. Lebowitz (Eds.) *Phase Transitions and Critical Phenomena* Vol. 11 Academic Press, New York
- Cuccoli, A., V. Tognetti, P. Verrucchi and R. Vaia (1992) Quantum thermodynamics of the easy-plane ferromagnetic chain. *Phys. Rev.*, **B46**, 11601
- Cullen, J.J. and D.P. Landau (1983) Monte Carlo studies of one-dimensional quantum Heisenberg and XY-models. *Phys. Rev.*, **B27**, 297
- Darriet, J. and L.P. Regnault (1993) The compound  $Y_2BaNiO_5$ : a new example of a Haldane-gap in  $S=1$  magnetic chain. *Solid State Commun.*, 86, 409
- Dekeyser, R. and G. Kamieniarz (1992) Effective field methods with correlations in magnetic systems. *J. Magn. Magn. Mat.*, **104-107**, 273
- Delica, T. and H. Leschke (1990) Formulation and numerical results of the transfer-matrix method for quantum spin chains. *Physica*, **A168**, 736
- Delica, T., W.J.M. de Jonge, K. Kopinga, H. Leschke and H.J. Mikeska (1991) Static properties of  $CsNiF_3$ : Comparison of numerical results, experimental data and predictions from soliton-bearing models. *Phys. Rev.*, **B44**, 11773
- Dupas, C. and J.P. Renard (1977) Low-temperature magnetic properties of three linear  $S=1$  ferromagnets with an easy plane anisotropy: TMNB, TMNC and  $CsNiF_3$ . *J. Phys. C: Solid State Phys.*, 10, 5057
- Ferrenberg, A.M. and D.P. Landau (1991) Critical behavior of the three-dimensional Ising model: a high resolution Monte Carlo study. *Phys. Rev.*, **B44**, 5081
- Fisher, M.E. and H. Au-Yang (1979) Inhomogeneous differential approximants for power series. *J. Phys. A: Math. Gen.*, **12**, 1677
- Gadet, V., M. Verdaguer, V. Briois, A. Gleizes, J.P. Renard, P. Beauvillain, C. Chappert, T. Goto, K. Le Dang and P. Veillet (1991) Structural and magnetic properties of  $(CH_3)_4NNi(NO_2)_3$ : a Haldane-gap system. *Phys. Rev.*, **B44**, 705
- Gatteschi, D., A. Caneschi, L. Pardi and R. Sessoli (1994) Large clusters of metal ions: the transition from molecular to bulk magnets. *Science*, **265**, 1054
- Gerling, R.W. and D.P. Landau (1990) Spin dynamics study of the classical ferromagnetic XY chain. *Phys. Rev.*, **B41**, 7139
- Grille, H., G. Kamieniarz and R.W. Gerling (1992) Spin dynamics of the classical easy-plane Heisenberg chain. *J. Magn. Magn. Mat.*, **104-107**, 1067
- Halperin, B.I. (1992) Quantum antiferromagnets in one and two dimensions. *J. Magn. Magn. Mat.*, **104-107**, 761
- Indekeu, J.O., A.Maritan and A.L.Stella (1982) Renormalization group recursions by mean-field approximations. *J. Phys. A: Math. Gen.* **15**, L291
- de Jongh, L.J. and A.R. Miedema (1974) Experiments on simple magnetic model systems. *Adv. Phys.*, **23**, 1

- Kakurai, K., M. Steiner and B. Dorner (1990) Study of the spin wave linewidth in 1D easy-plane ferromagnet using neutron polarization analysis. *Europhys. Lett.*, **12**, 653
- Kamieniarz, G., F. Mallezie and R. Dekeyser (1988) Magnetization and correlation length of the easy-plane ferromagnetic chain: numerical analysis and application to  $(\text{C}_6\text{H}_{11}\text{NH}_3)\text{CuBr}_3$ . *Phys. Rev.*, **B38**, 6941
- Kamieniarz, G. and H.W.J. Blöte (1993a) Universal ratio of magnetization moments in two-dimensional Ising model. *J. Phys. A: Math. Gen.*, 26, 201
- Kamieniarz, G. and H. Blöte (1993b) The non-interacting hard-square lattice gas: Ising universality. *J. Phys. A: Math. Gen.*, 26, 6679
- Kamieniarz, G., G. Musial and R. Dekeyser (1994) Effective field methods for magnetic systems. *Acta Phys. Polon.*, **A85**, 413
- Kamieniarz, G. and R. Matysiak (1996a), in preparation
- Kamieniarz, G., G. Musial and R. Dekeyser (1996b), in preparation
- Klümper, A. and P.A. Pearce (1993) New results for exactly solvable critical RSOS models and vertex models in two dimensions. *Physica*, **A194**, 397
- Kopinga, K., J. Emmen, G.C. de Vries, L.F. Lemmens and G. Kamieniarz (1988) Comparison between experiment and numerical calculations on  $S=1/2$  Heisenberg-XY ferromagnetics chains. *J. de Physique*, C8, 1451
- Kopinga, K., T. Delica and H. Leschke (1989) Static properties of an easy-plane ferromagnetics  $S=1/2$  chain: comparison of numerical results and experimental data on  $(\text{C}_6\text{H}_{11}\text{NH}_3)\text{CuBr}_3$ . *Phys. Rev.*, **B40**, 7239
- Kopinga, K., T. Delica, H. Leschke and I. Riedel (1993) Static properties of a ferromagnetic  $S=1/2$  chain system with orthorhombic exchange anisotropy: comparison of numerical results and experimental data on  $(\text{CgITuNH}_3)\text{CuCl}_3$ . *Phys. Rev.*, **B47**, 5447
- Landau, D.P. (1994) Computer simulation studies of critical phenomena. *Physica*, A205, 41
- Le Guillou, J.C. and J. Zinn-Justin (1980) Critical exponents from field theory. *Phys. Rev.*, **B21**, 3976
- Liu, A.J. and M.E. Fisher (1989) The three-dimensional Ising model revisited numerically. *Physica*, **A156**, 35
- Livet, F. (1991) The cluster updating Monte Carlo algorithm applied to the 3D Ising problem. *Europhys. Lett.*, **16**, 139
- Manousakis, E. (1991) The spin- $\frac{1}{2}$  Heisenberg antiferromagnet on a square lattice and its applications to the cuprous oxides. *Rev. Mod. Phys.*, 63, 1
- Mikeska, H.J. (1978) Solitons in a one-dimensional magnet with an easy plane. *J. Phys. G: Solid State Phys.*, **11**, L29

- Mikeska, H.J. and M. Steiner (1991) Solitary excitations in one-dimensional magnets. *Adv. Phys.*, **40**, 191
- Morra, R.M., R.M. Armstrong, W.J.L. Buyers and H. Hirakawa (1988) Spin dynamics and the Haldane gap in the spin-1 quasi-one-dimensional antiferromagnet  $CsNiCl_3$ . *Phys. Rev.*, **B38**, 543
- Moses, D., E. Ehrenfreund, J. Makovsky and H. Shechter (1977) Magnetic specific heat of the nearly one-dimensional antiferromagnet  $CsNiCl_3$ . *J. Phys. C: Solid State Phys.*, **10**, 433
- de Neef, T. (1976) Thermodynamics of magnetic chains with  $S \leq 5/2$ . *Phys. Rev.*, **B13**, 4141
- Niemeijer, Th. and J.M.J. van Leeuwen (1976) Renormalization theory for Ising-like spin systems. In C. Domb and M.S. Green (Eds.) *Phase Transitions and Critical Phenomena*, Vol. 6, Acad. Press, London, New York and San Francisco, p. 425
- Nickel, B.G. and J.J. Rehr (1990) High-Temperature Series for Scalar Field Lattice Models: Generations and Analysis *J. Stat. Phys.*, **61**, 1
- Pawlicki, P., G. Kamieniarz and J. Rogiers (1995) Phase diagram of the extended Ashkin-Teller model. *J. Magn. Magn. Mat.*, **140-144**, 1471
- Pearce, P.A. and K.A. Seaton (1990) The off-critical integrable Ashkin-Teller model. *J. Phys. A: Math. Gen.*, **23**, 1191
- Privman, V. and M.E. Fisher (1984) Universal critical amplitudes in finite-size scaling. *Phys. Rev.*, **B30**, 322
- Racz, Z. (1980) Phase boundary of Ising antiferromagnets near  $H = H_c$  and  $T = 0$ : Results from hard-core lattice gas calculations. *Phys. Rev.*, **B21**, 4012
- Ramirez, A.P. and W.P. Wolf (1985) Specific heat of  $CsNiF_3$ . *Phys. Rev.*, **B32**, 1639
- Ramirez, A.P., S.-W. Cheong and M.L. Kaplan (1994) Specific heat of defects in Haldane systems  $Y_2BaNiO_5$  and  $NENP$ : absence of the spin-1/2 excitations. *Phys. Rev. Lett.*, **72**, 3108
- Rosengren, A. (1986) On the combinatorial solution of the Ising model. *J. Phys. A: Math. Gen.*, **19**, 1709
- Steiner, M., J. Villain and C.G. Windsor (1976) Theoretical and experimental studies on one-dimensional magnetic systems. *Adv. Phys.*, **25**, 1
- Steiner, M. and J.K. Kjems (1977) Spin waves in  $CsNiF_3$  with an applied magnetic field. *J. Phys. C: Solid State Phys.*, **10**, 2665
- Steiner, M., K. Kakurai and J.K. Kjems (1983) Experimental Study of the Spindynamics in the 1-D Ferromagnet with Planar Anisotropy:  $CsNiF_3$  in an External Magnetic Field. *Z. Phys.*, **B53**, 117

Suzuki M. (1993) Quantum Monte Carlo methods - recent developments. *Physica*, **A194**, 432

Swendsen, R.H. and J.-S. Wang (1988) Nonuniversal Critical Dynamics in Monte Carlo Simulations. *Phys. Rev. Lett.*, **58**, 86

Weng, C.J. (1968) Ph. D. Thesis, Cornege Institute of Technology

Wolff, U. (1989) Collective Monte Carlo Updating for Spin System. *Phys. Rev. Lett.*, **62**, 361

Wood, D.W. and M. Goldfinch (1980) Vertex models for the hard-square and hard hexagon gases, and critical parameters from the scaling transformations. *J. Phys. A: Math. Gen.*, **13**, 2781